Effect of electronic structure of energy transfer in bimetallic Ru(II)/Os(II) complexes

Weijun Dai, Shiwen Yu, Ci Kong, Defang Zhao, Chixian He, Zining Liu, Jianwei Dong, Jian-Jun Liu*, Feixiang Cheng*

College of Chemistry and Environmental Science, Qujing Normal University, Qujing 655011

E-mail: jjliu302@163.com; chengfx2019@163.com

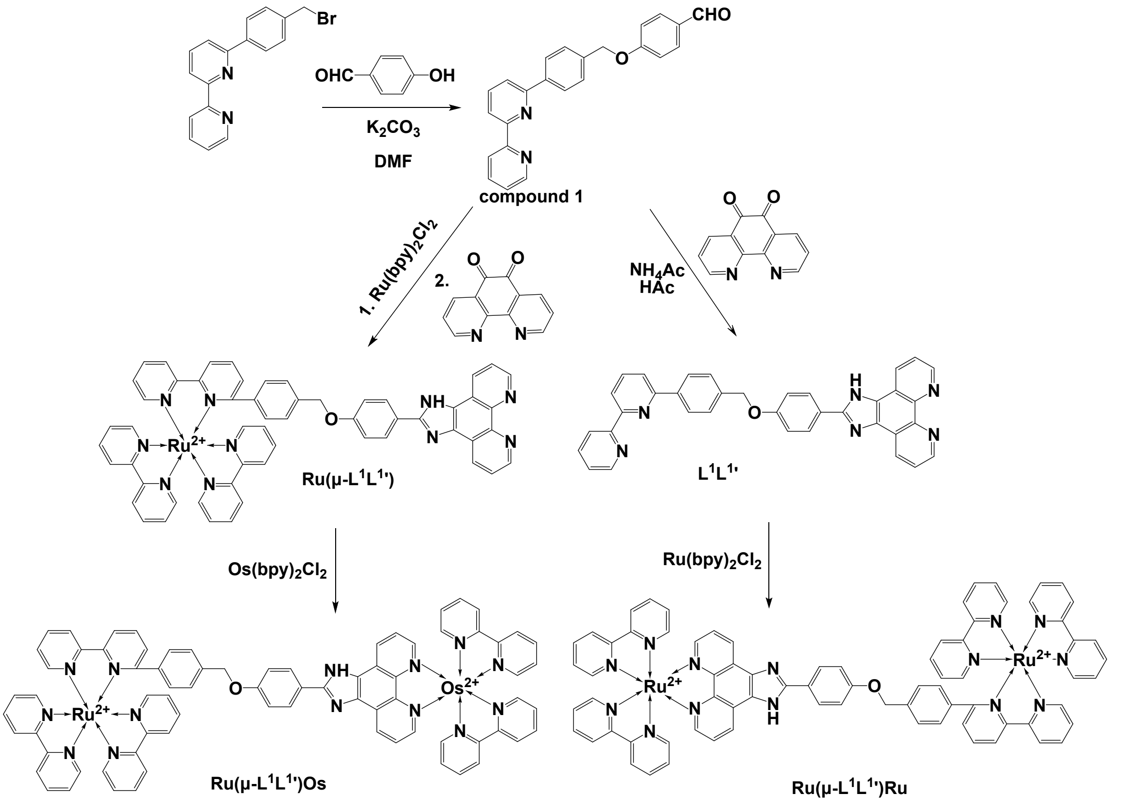

Scheme S1. Chemical structures of the target monometallic Ru(L^{1}L$^{1'}$), homometallic Ru(μ-L^{1}L$^{1'}$)Ru and heterometallic Ru(μ-L^{1}L$^{1'}$)Os complexes.

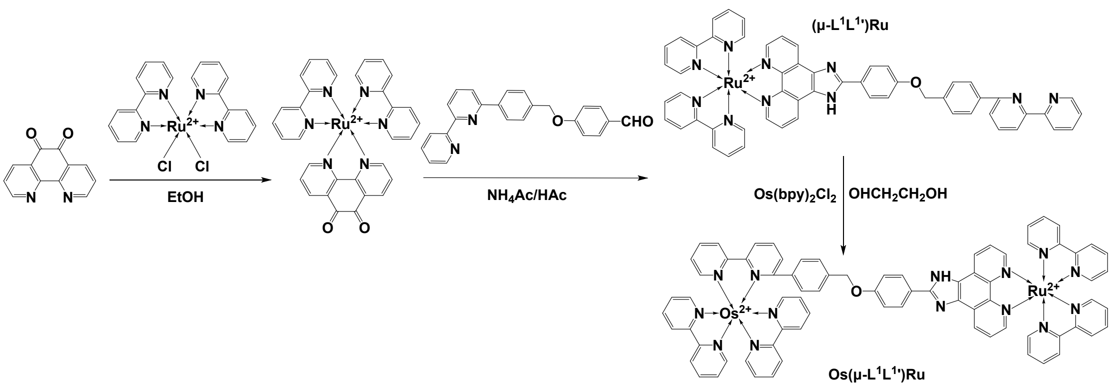

Scheme S2. Chemical structures of the target monometallic (μ-L^{1}L$^{1'}$)Ru, heterometallic Os(μ-L^{1}L$^{1'}$)Ru complexes.

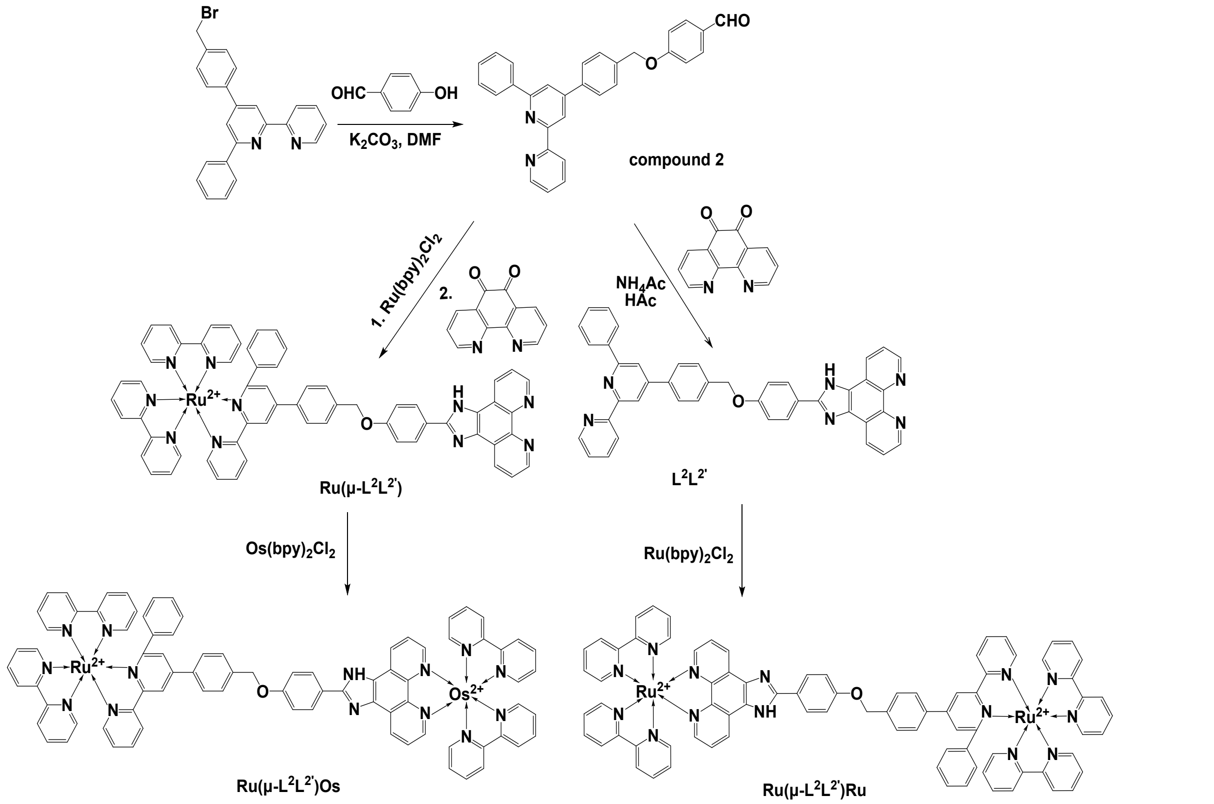

Scheme S3. Chemical structures of the target monometallic Ru(μ-L^{2}L$^{2'}$), homometallic Ru(μ-L^{2}L$^{2'}$)Ru, heterometallic Ru(μ-L^{2}L$^{2'}$)Os complexes.

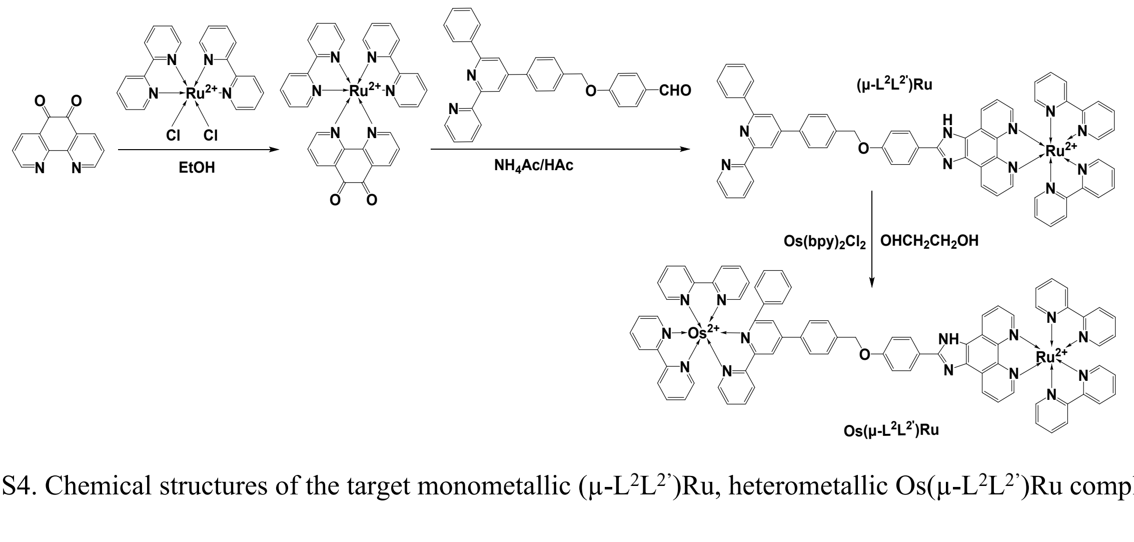

Scheme S4. Chemical structures of the target monometallic (μ-L^{2}L$^{2'}$)Ru, heterometallic Os(μ-L^{2}L$^{2'}$)Ru complexes.

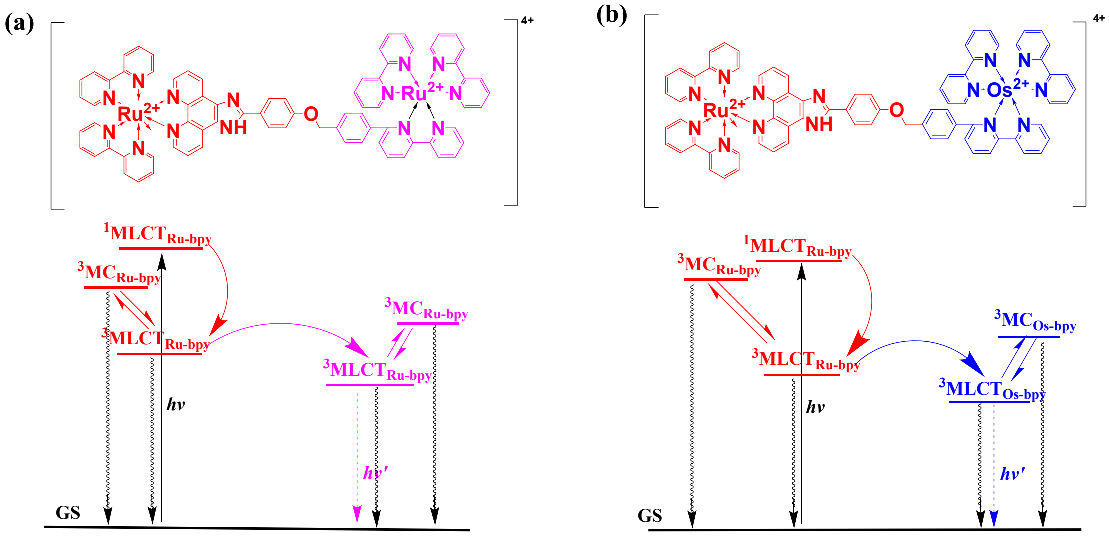

Figure S1. Energy level diagrams of complexes Ru(μ-L^{1}L$^{1'}$)Ru (a), Os(μ-L^{1}L$^{1'}$)Ru (b). The full line, dotted line and curved line represent excitation, luminescence and non-radiative decay, respectively.

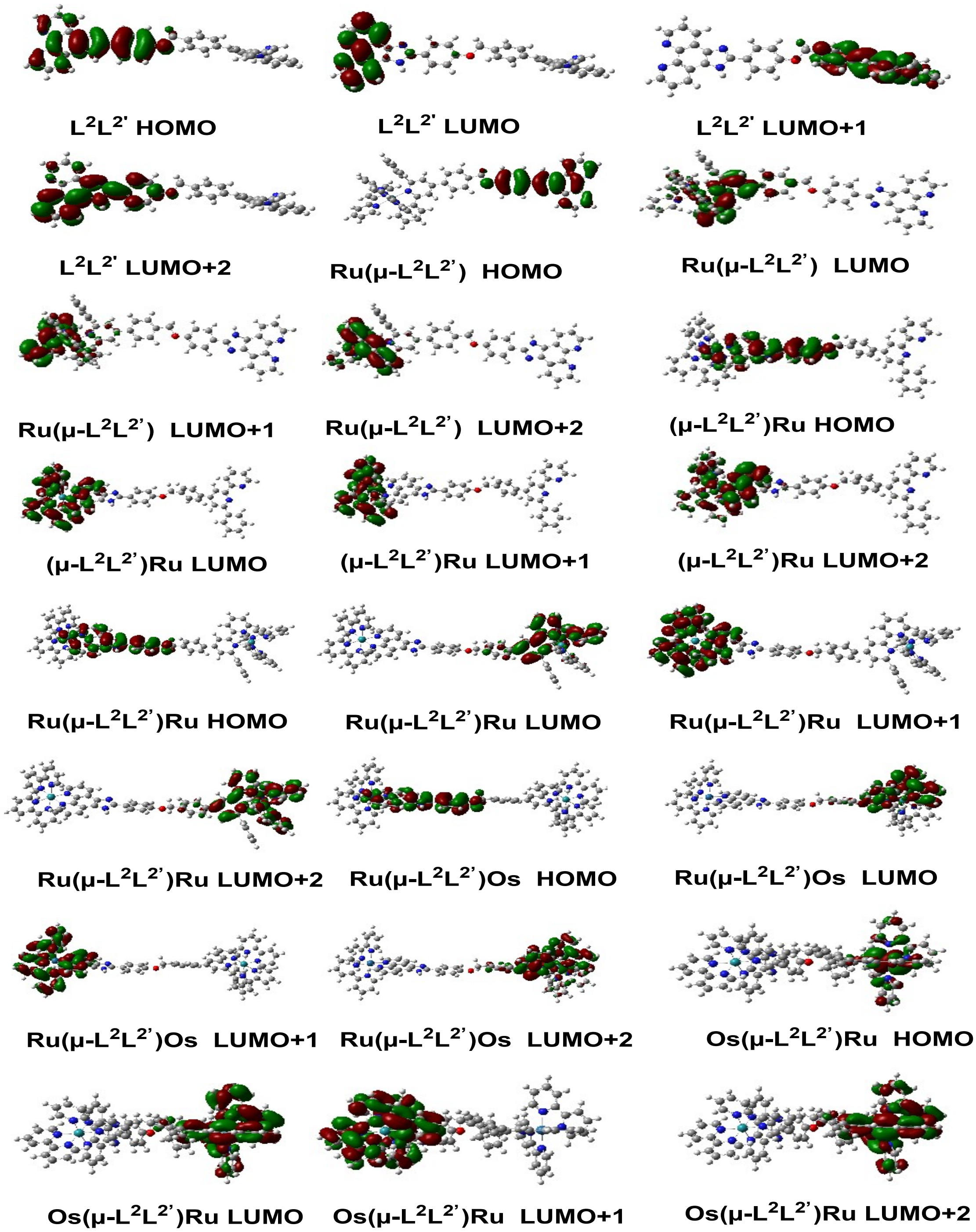

Figure S2. The HOMO and the LUMOs of the complexes containing bridging ligand $L^2L^{2'}$

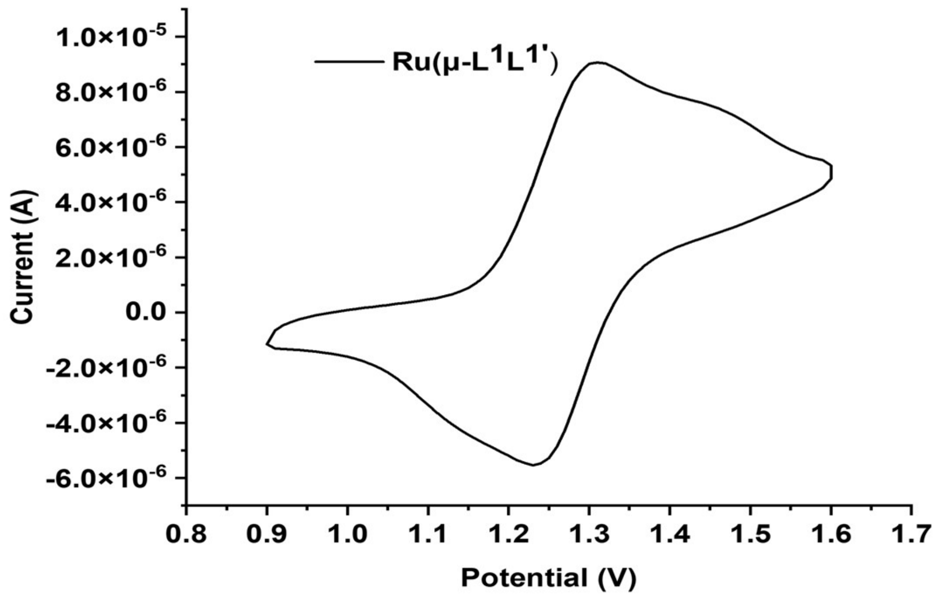

Figure S3. Oxidation cyclic voltammetry of complex Ru(μ-$L^1L^{1'}$)

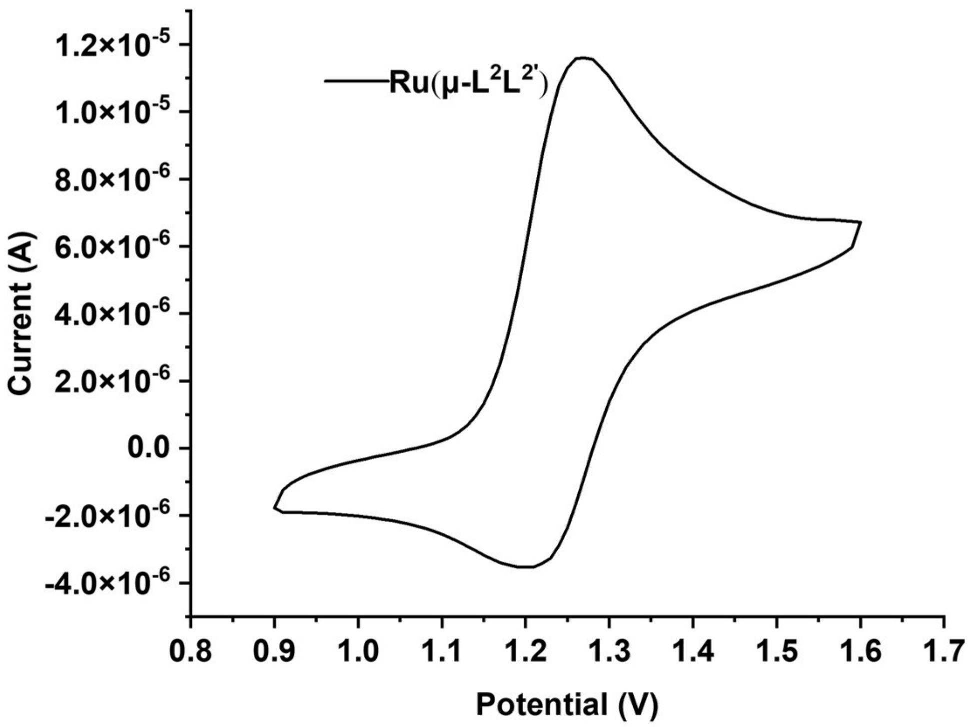

Figure S4. Oxidation cyclic voltammetry of complex Ru(μ-$L^2L^{2'}$)

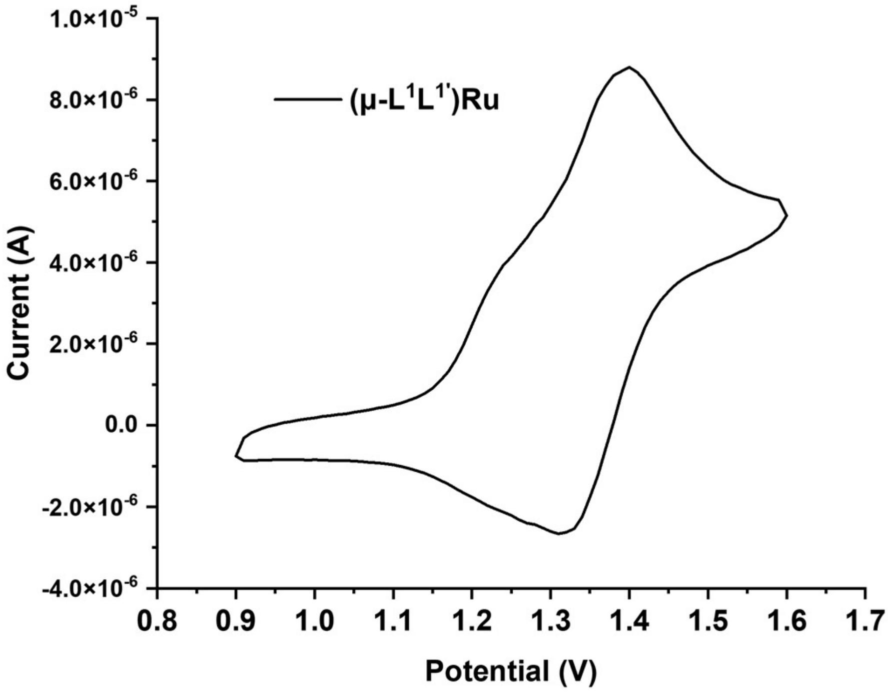

Figure S5. Oxidation cyclic voltammetry of complex (μ-$L^1L^{1'}$)Ru

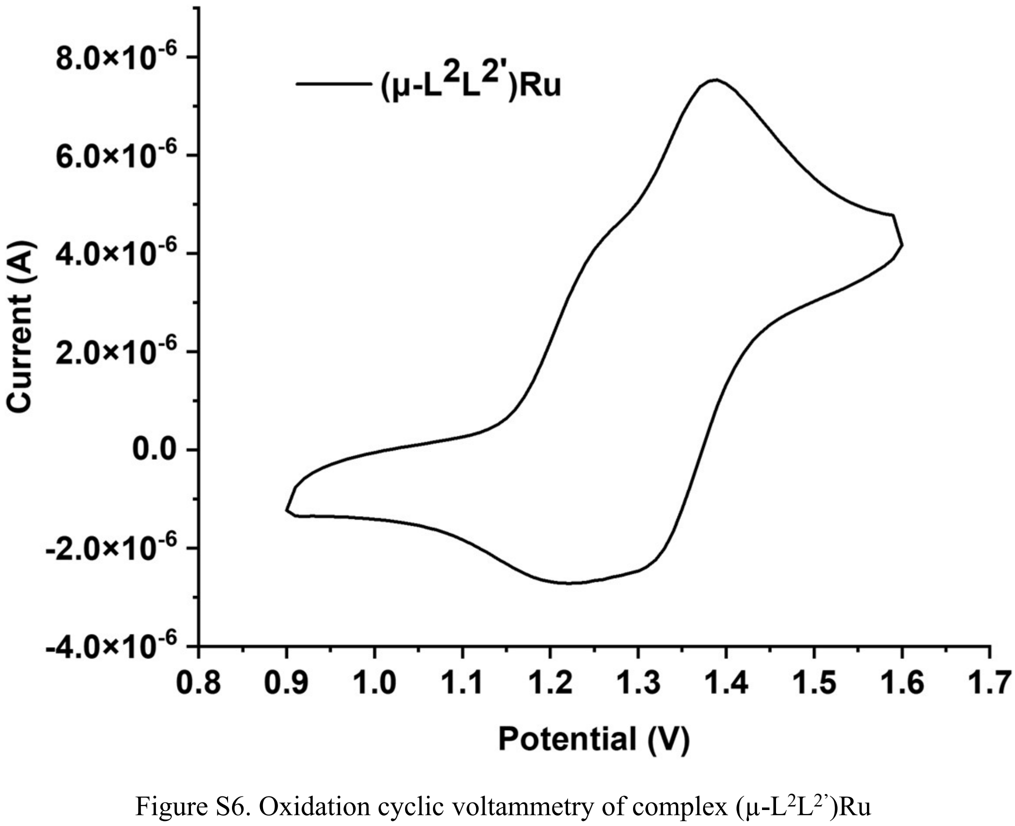

Figure S6. Oxidation cyclic voltammetry of complex (μ-$L^2L^{2'}$)Ru

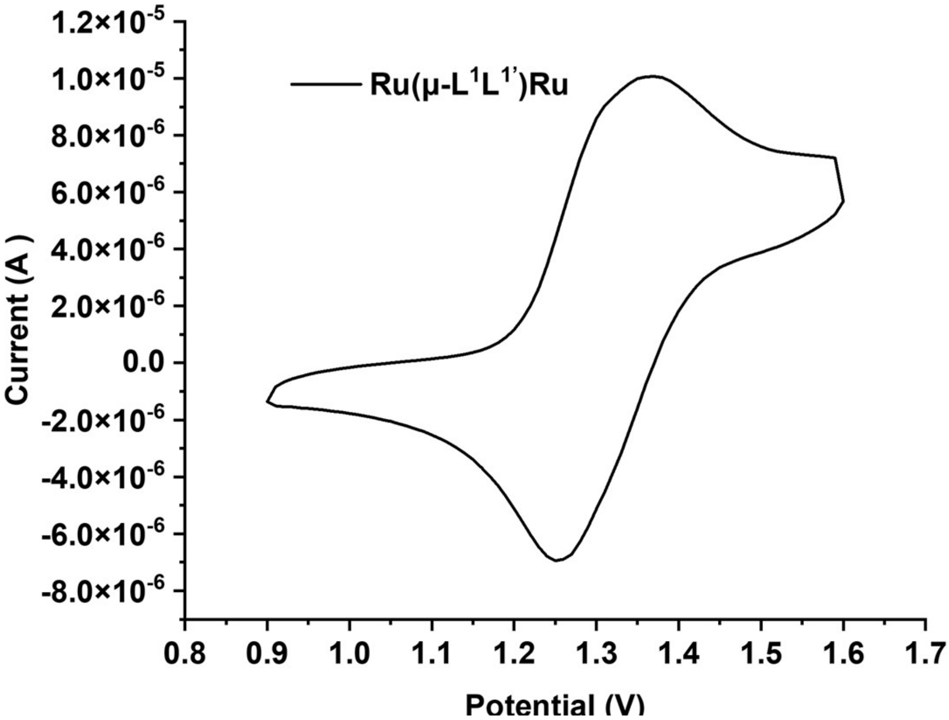

Figure S7. Oxidation cyclic voltammetry of complex Ru(μ-$L^1L^{1'}$)Ru

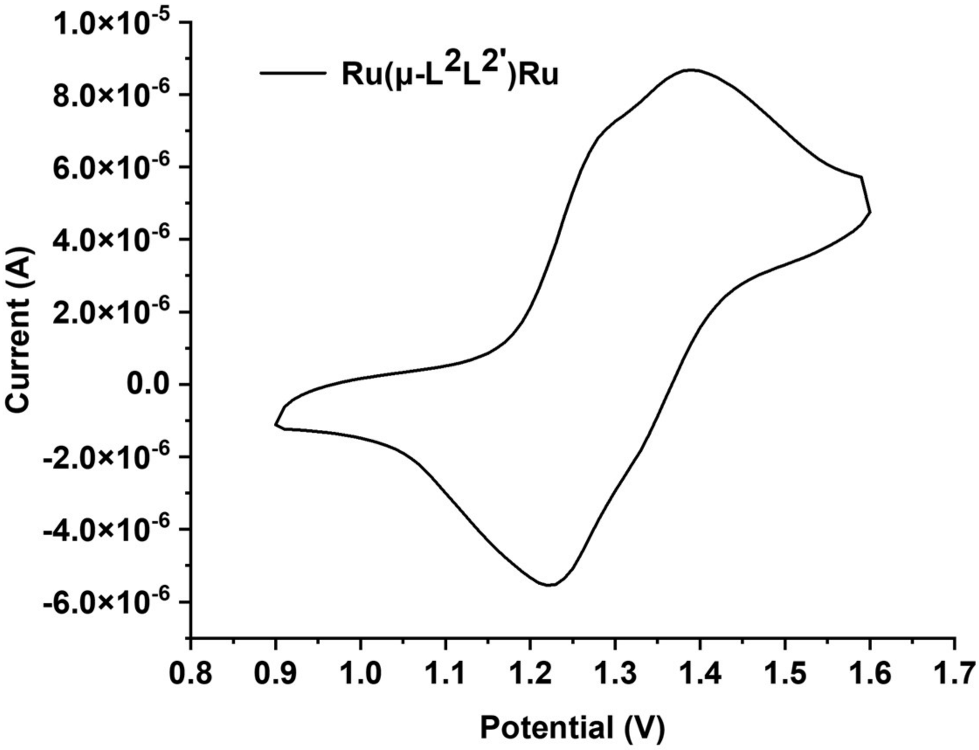

Figure S8. Oxidation cyclic voltammetry of complex Ru(μ-$L^2L^{2'}$)Ru

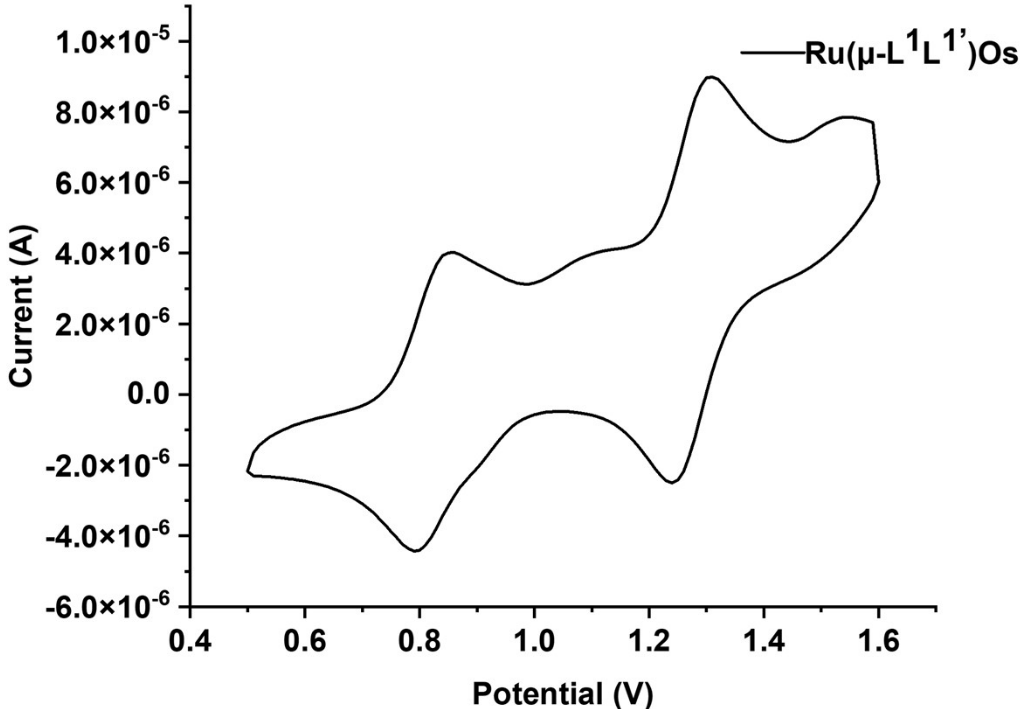

Figure S9. Oxidation cyclic voltammetry of complex Ru(μ-$L^1L^{1'}$)Os

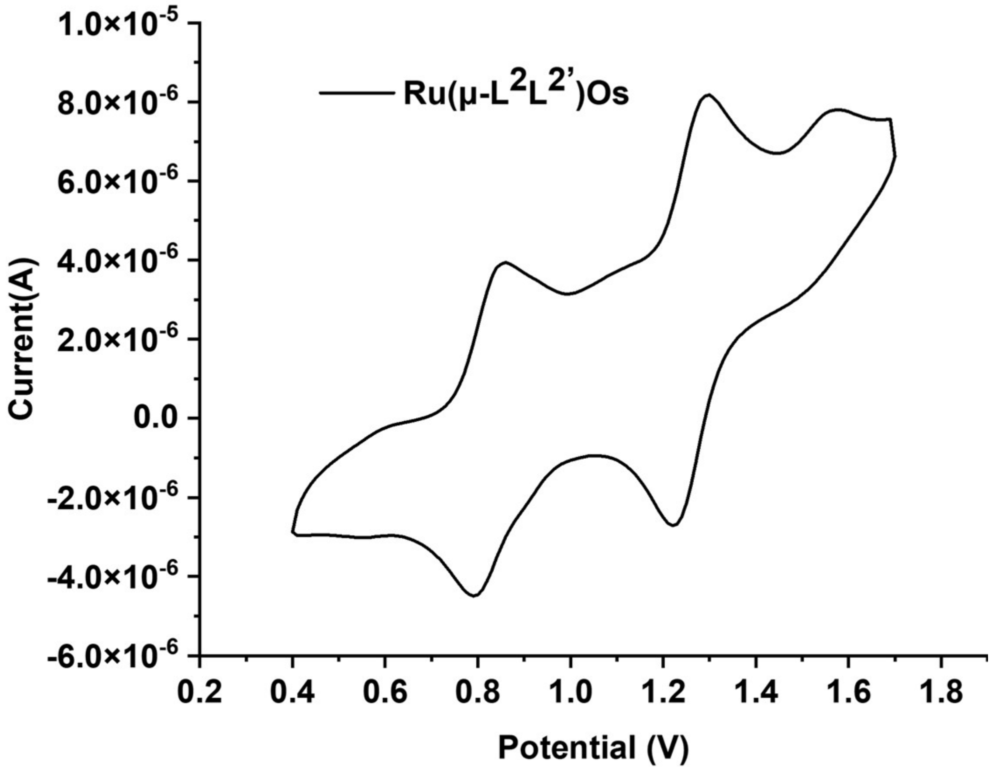

Figure S10. Oxidation cyclic voltammetry of complex Ru(μ-$L^2L^{2'}$)Os

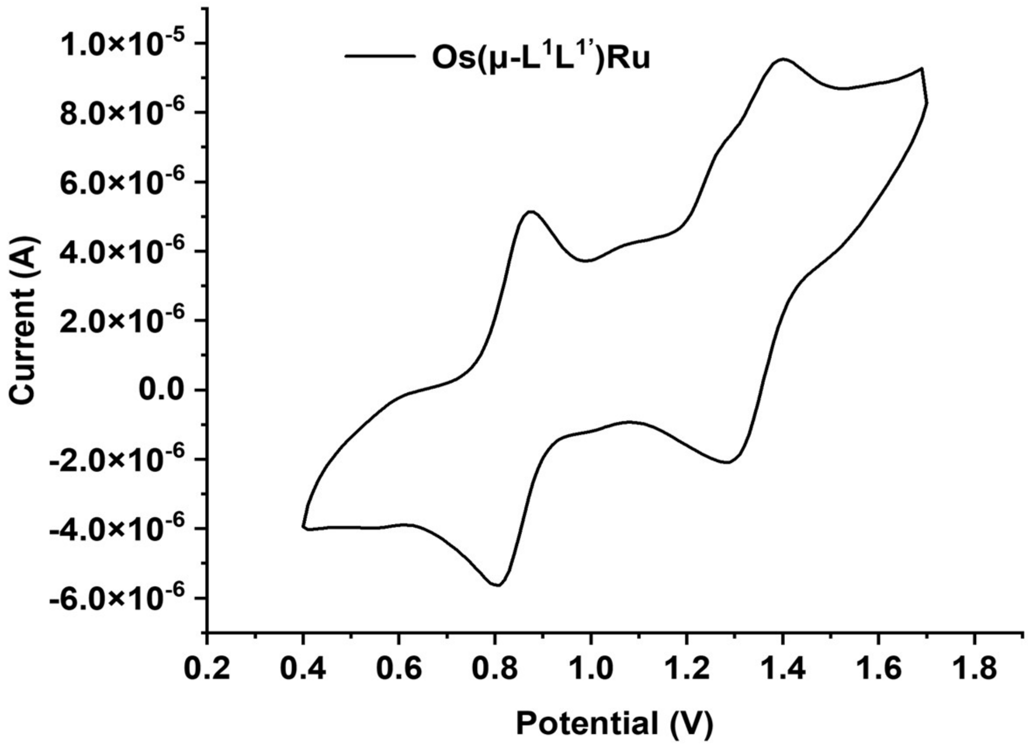

Figure S11. Oxidation cyclic voltammetry of complex Os(μ-$L^1L^{1'}$)Ru

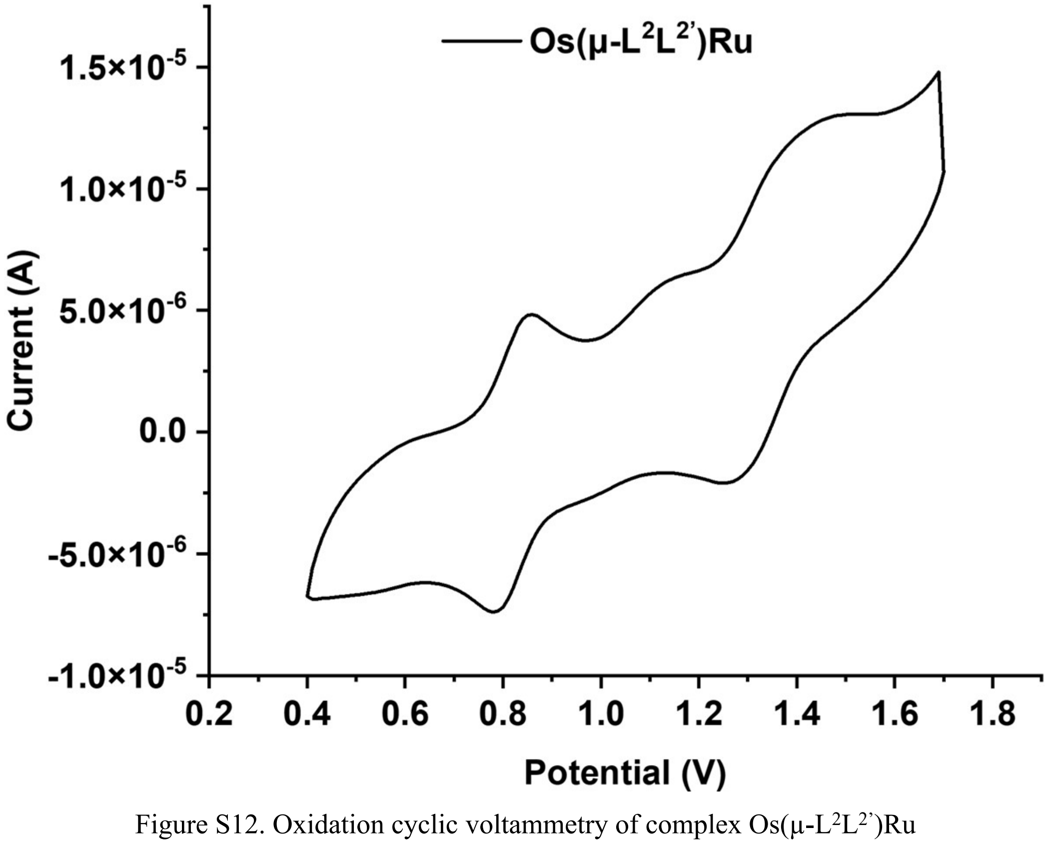

Figure S12. Oxidation cyclic voltammetry of complex Os(μ-$L^2L^{2'}$)Ru

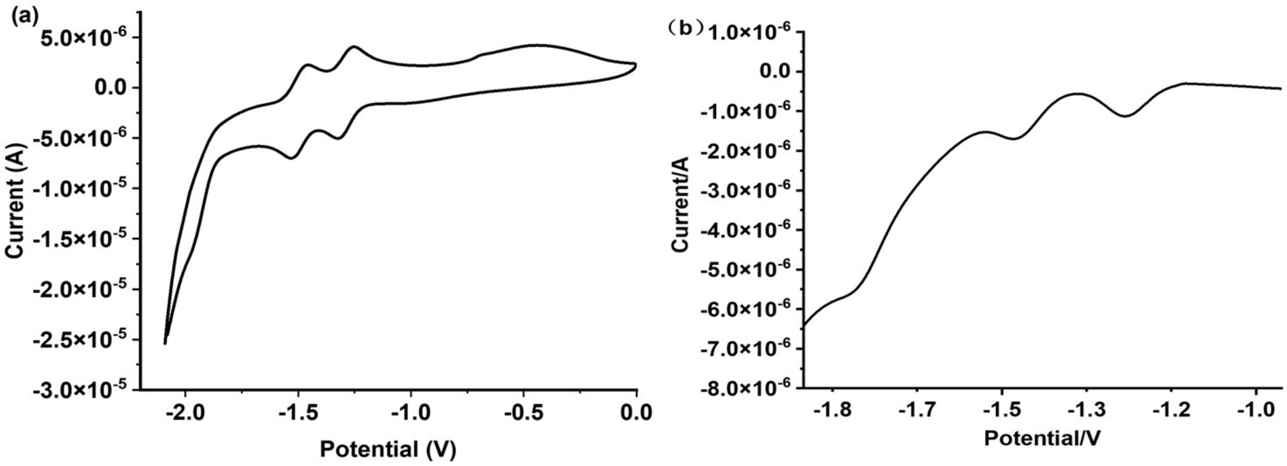

Figure S13. Reduction cyclic voltammetry of complex Ru(μ-$L^1L^{1'}$)

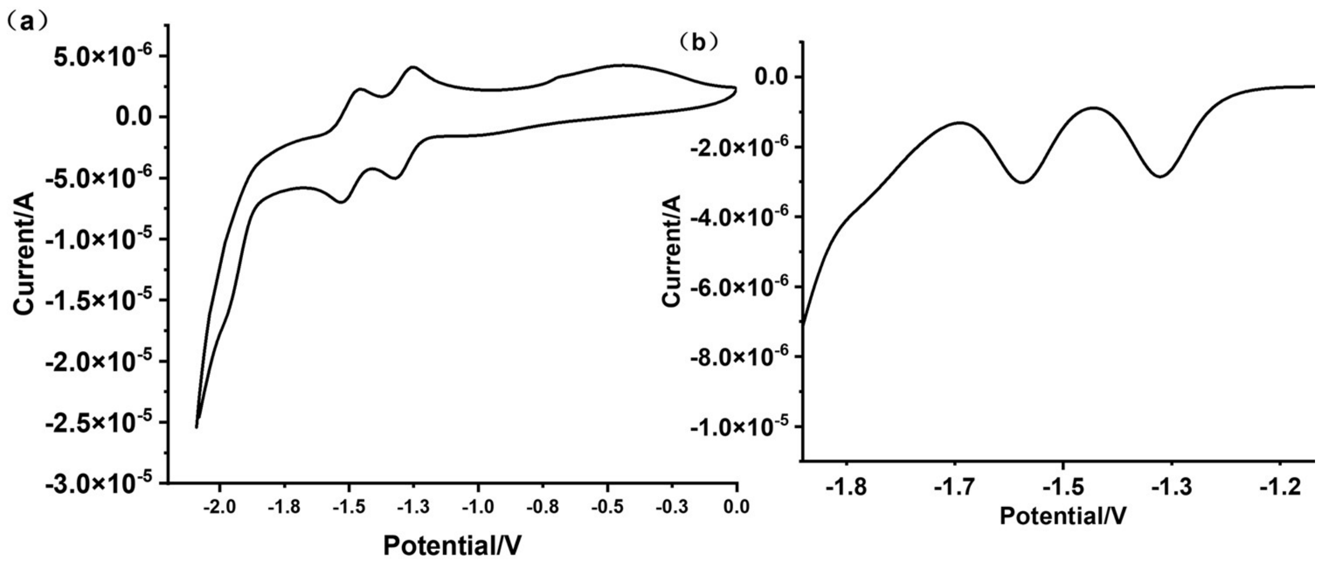

Figure S14. Reduction cyclic voltammetry of complex (μ-$L^1L^{1'}$)Ru

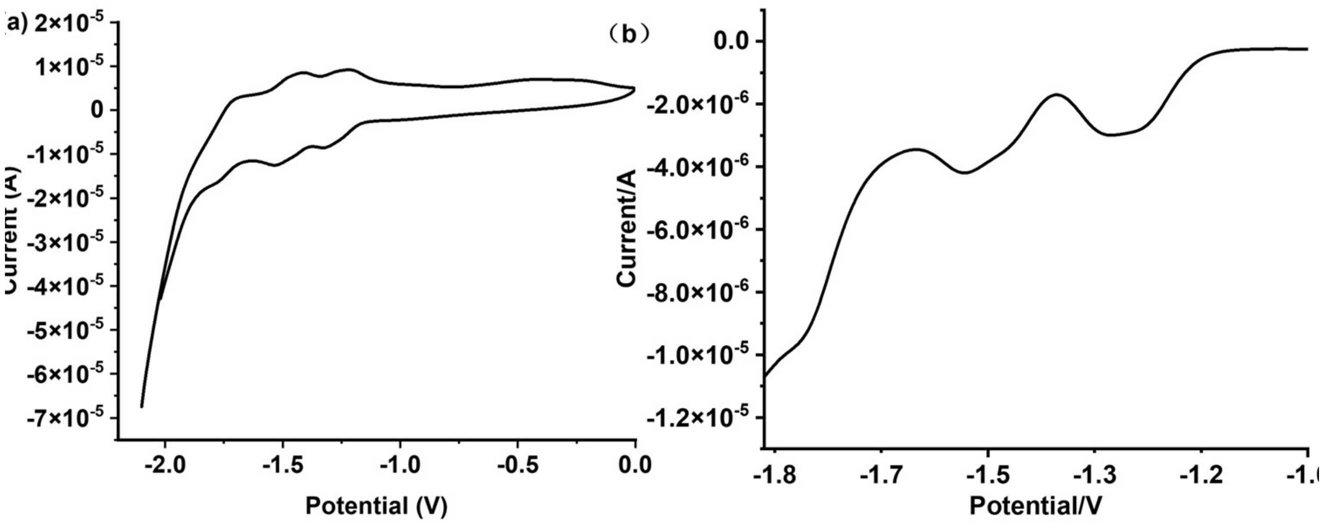

Figure S15. Reduction cyclic voltammetry of complex Ru(μ-L[1]L[1']')Ru

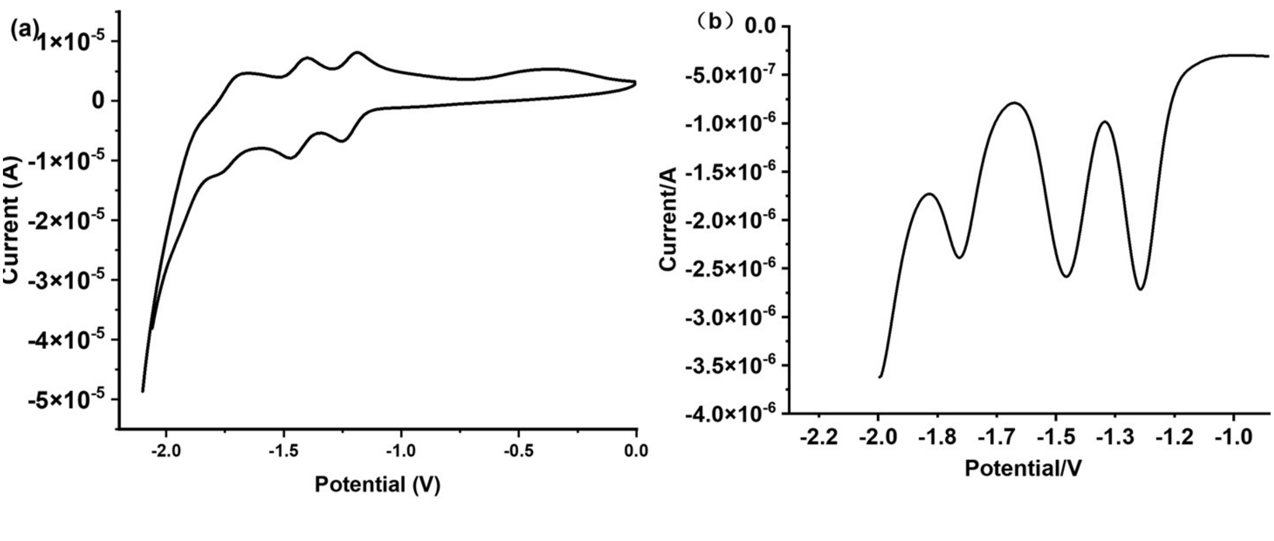

Figure S16. Reduction cyclic voltammetry of complex Ru(μ-L[1]L[1']')Os

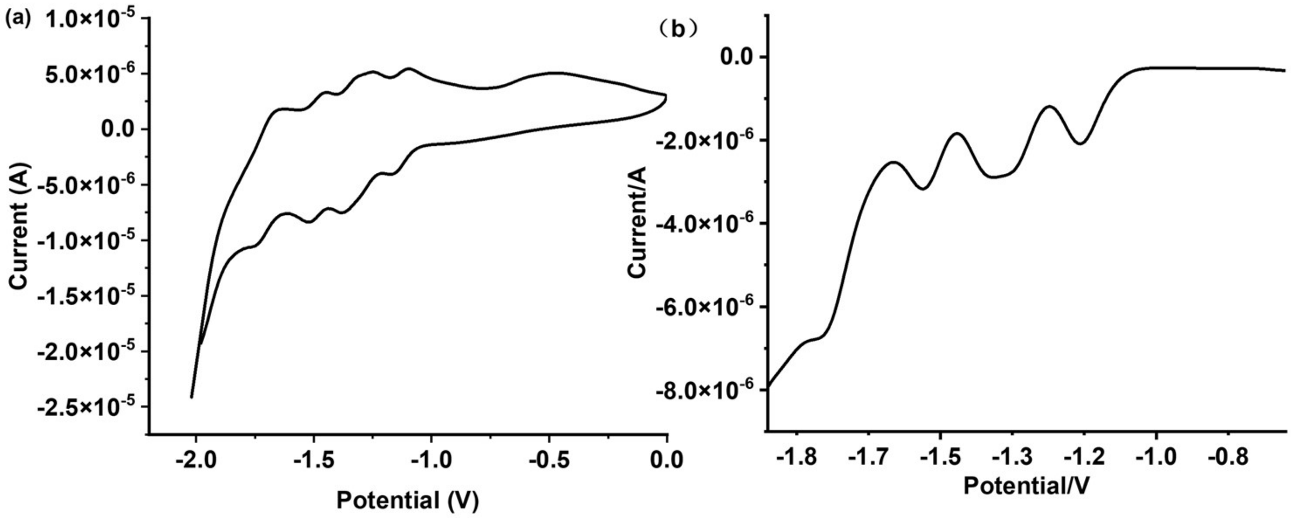

Figure S17. Reduction cyclic voltammetry of complex Os(μ-$L^1L^{1'}$)Ru

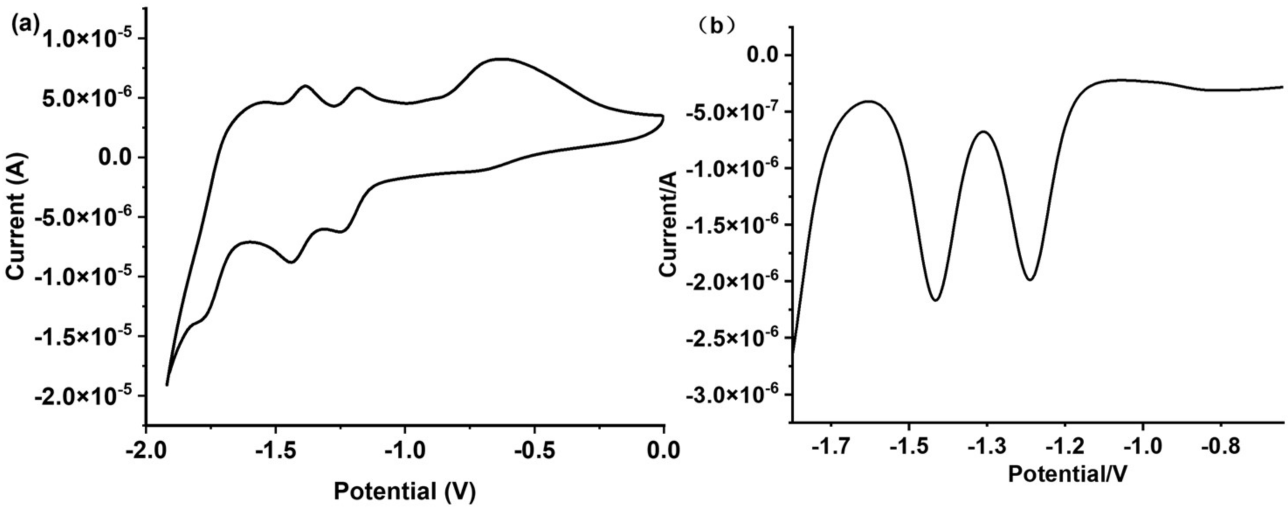

Figure S18. Reduction cyclic voltammetry of complex Ru(μ-$L^2L^{2'}$)

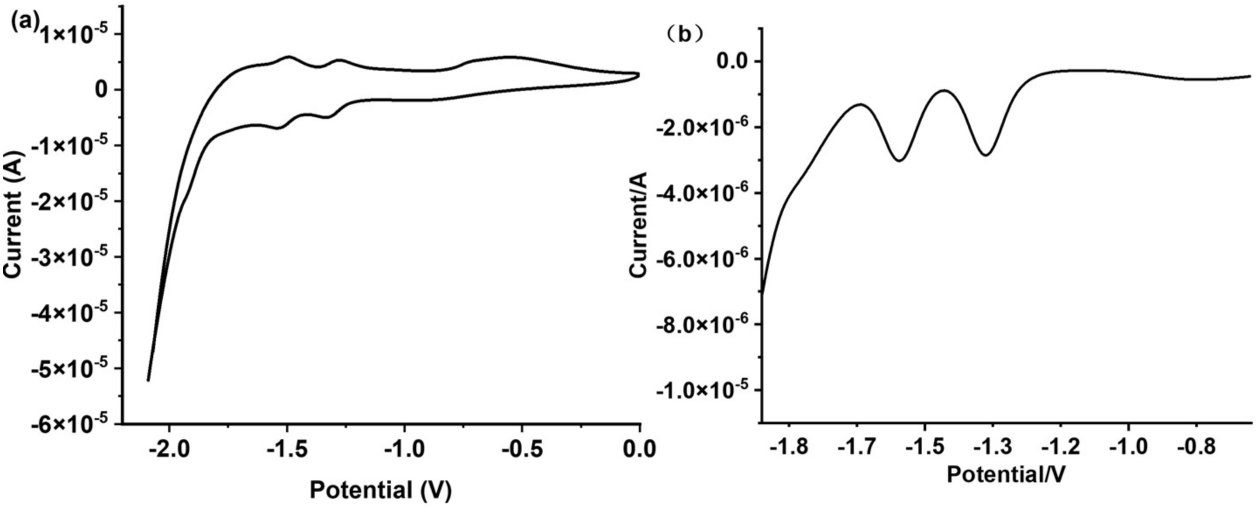

Figure S19. Reduction cyclic voltammetry of complex (μ-$L^2L^{2'}$)Ru

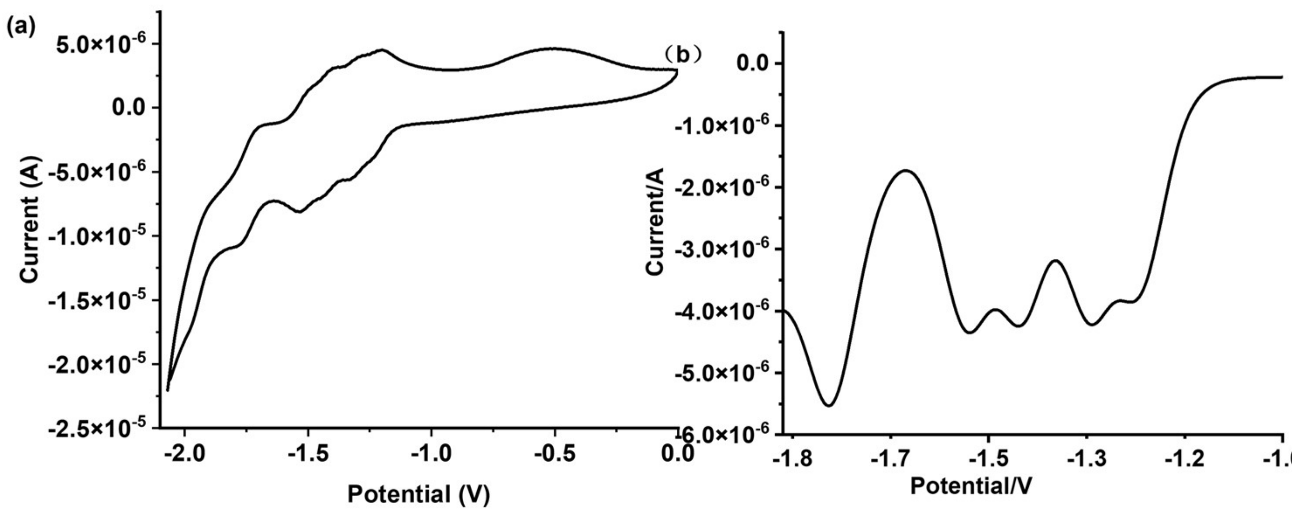

Figure S20. Reduction cyclic voltammetry of complex Ru(μ-$L^2L^{2'}$)Ru

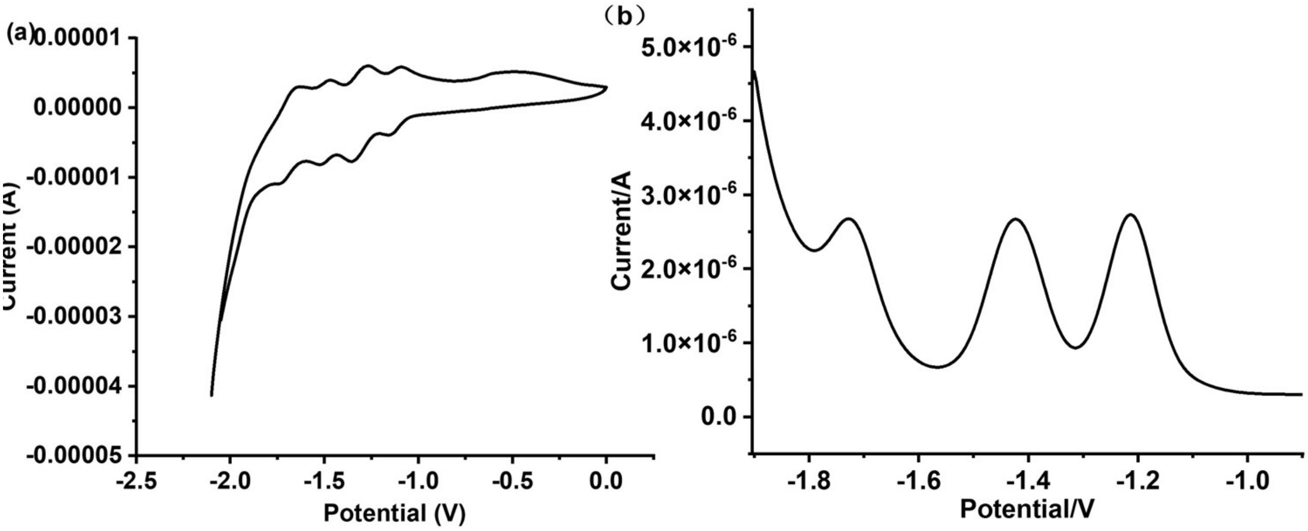

Figure S21. Reduction cyclic voltammetry of complex Ru(μ-$L^2L^{2'}$)Os

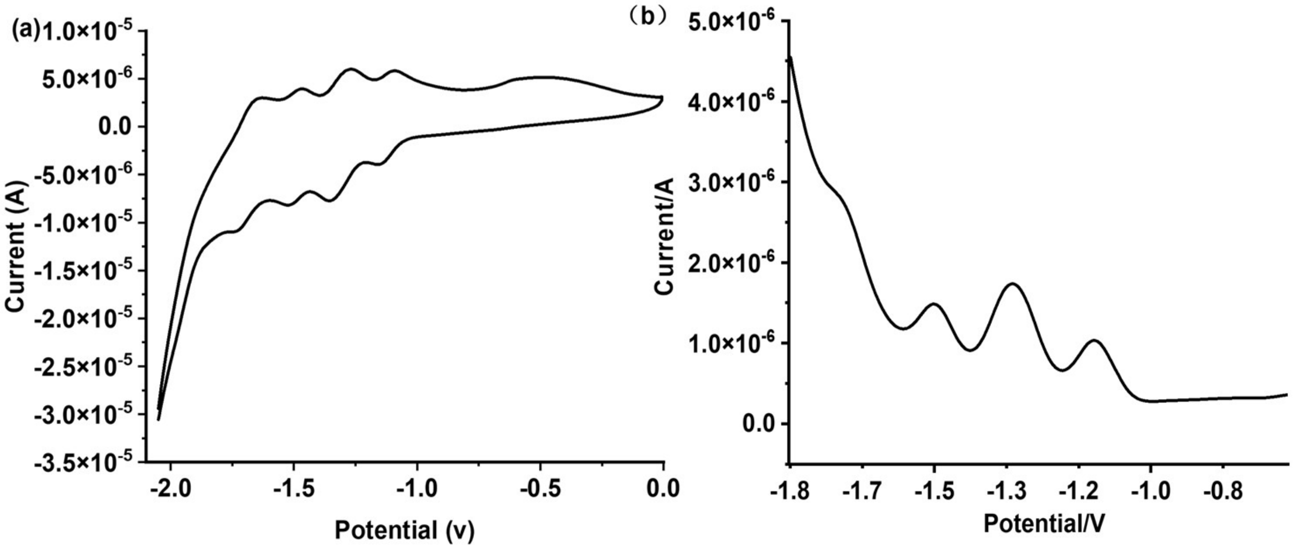

Figure S22. Reduction cyclic voltammetry of complex Os(μ-$L^2L^{2'}$)Ru

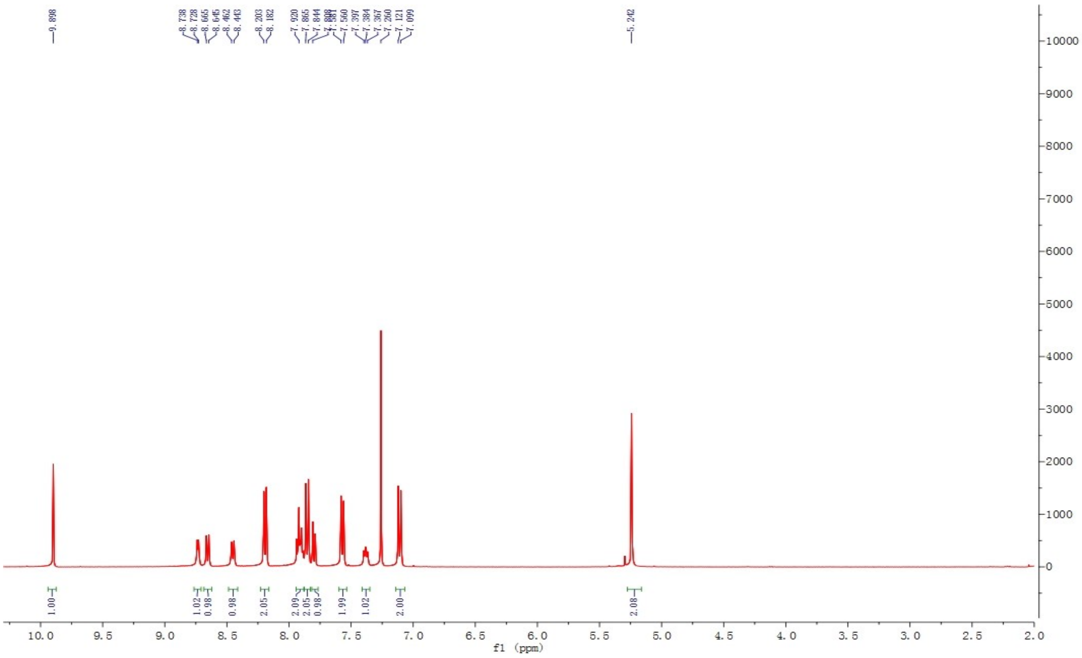

Figure S23. ^{1}H NMR (400 MHz, $CDCl_3$) spectrum of compound 1

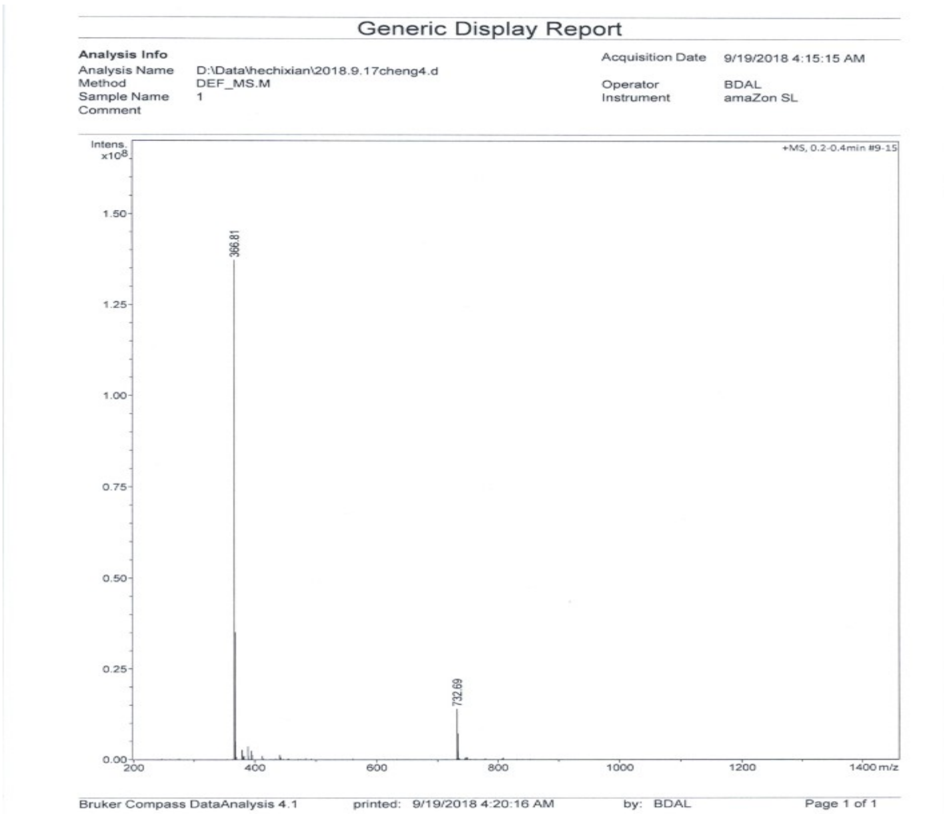

Figure S24. ESI-MS of compound 1

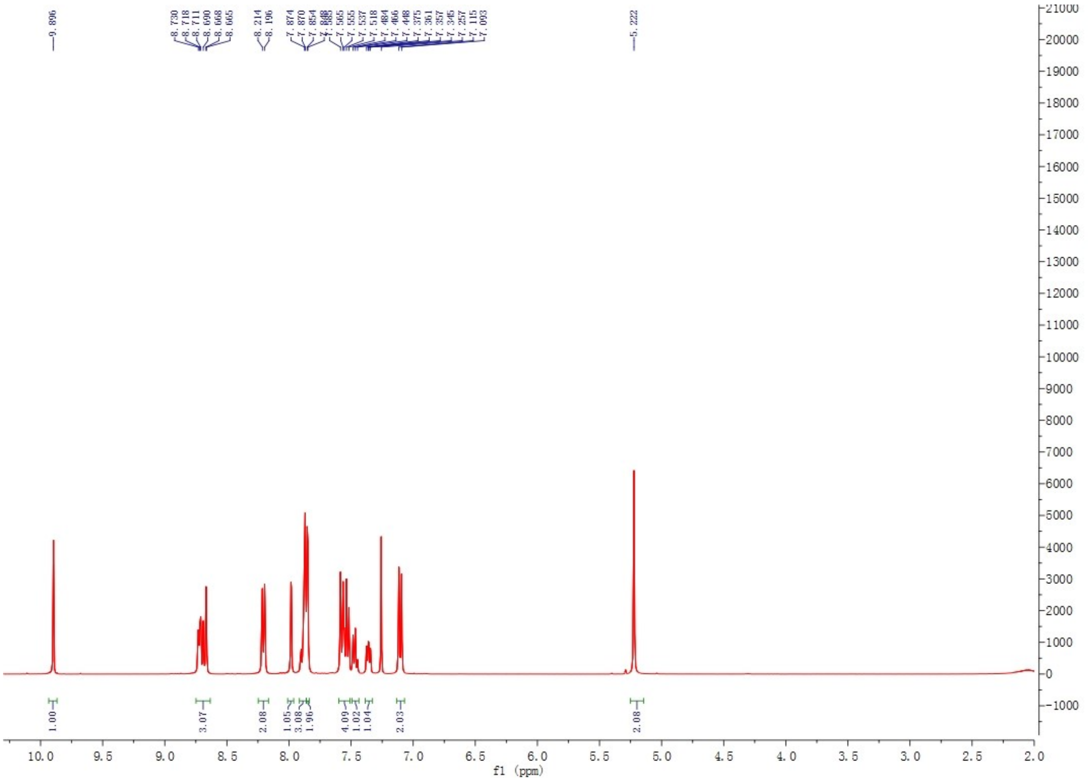

Figure S25. ^{1}H NMR (400 MHz, $CDCl_3$) spectrum of compound 2

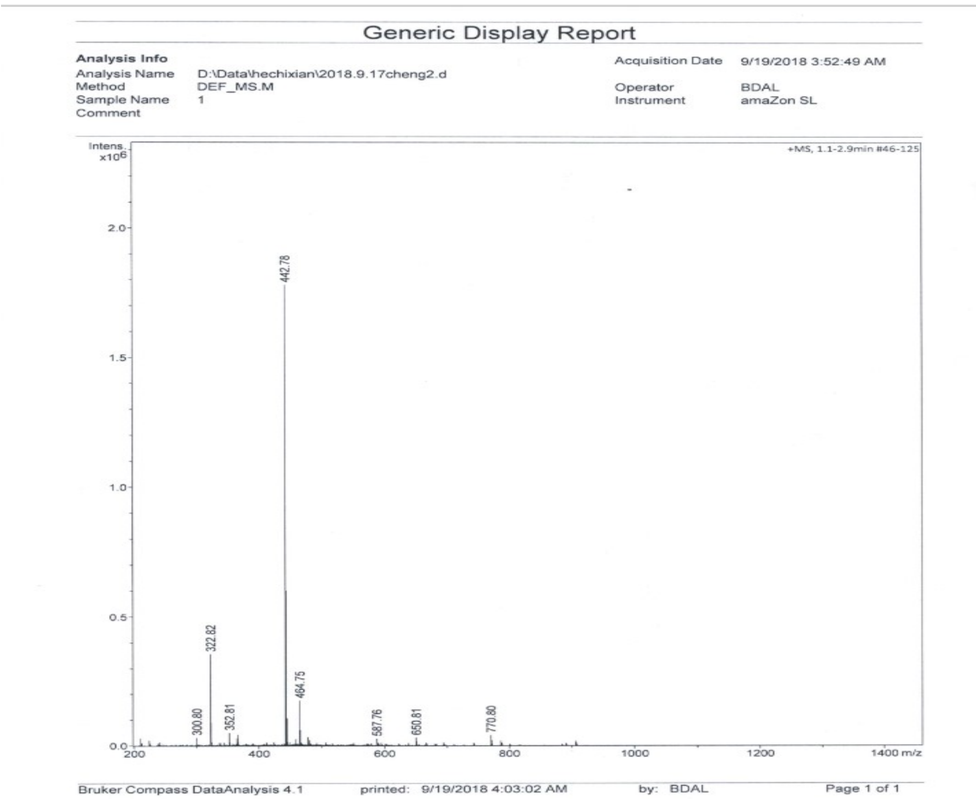

Figure S26. ESI-MS of compound 2

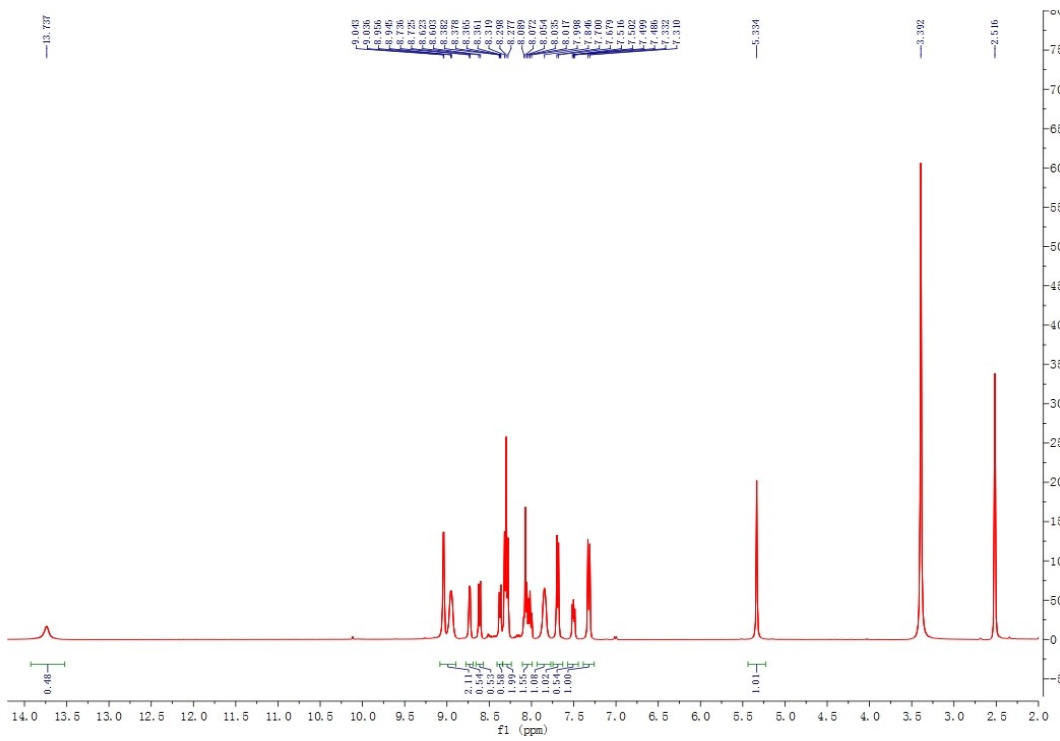

Figure S27. ^{1}H NMR (400 MHz, DMSO-d_6) spectrum of ligand $L^1L^{1'}$

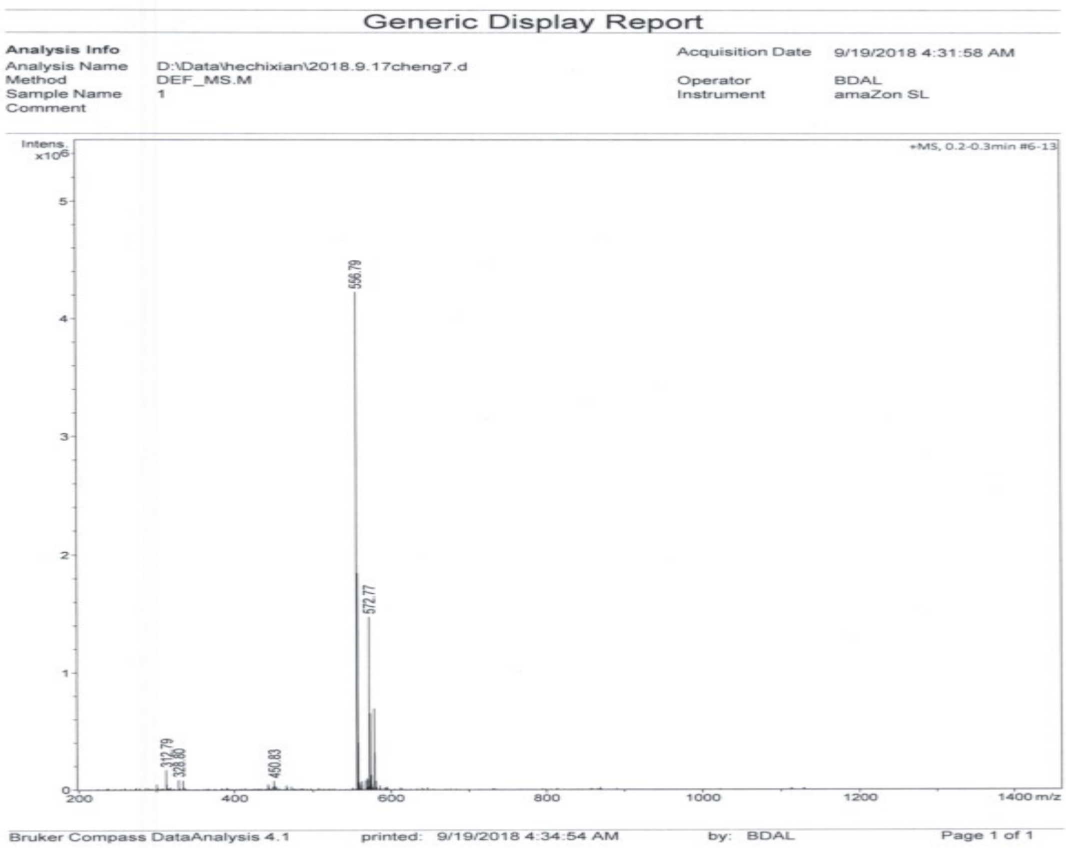

Figure S28. ESI-MS of ligand $L^1L^{1'}$

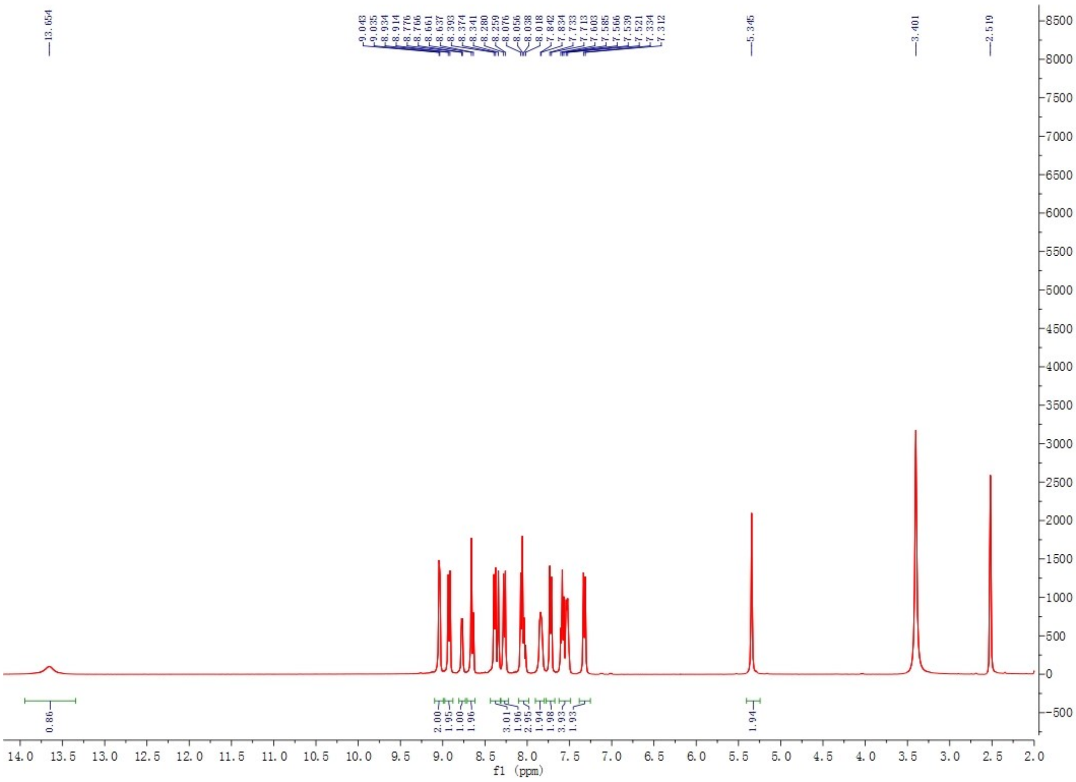

Figure S29. ^1H NMR (400 MHz, DMSO-d_6) spectrum of ligand $L^2L^{2'}$

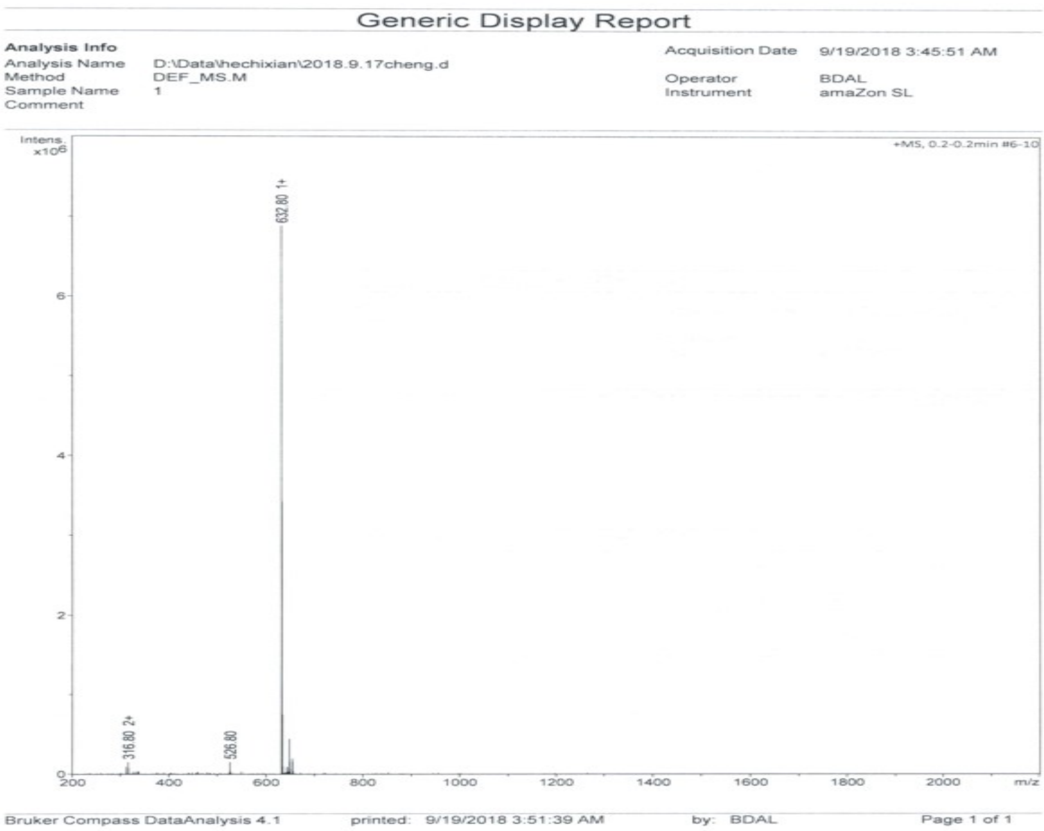

Figure S30. ESI-MS of ligand $L^2L^{2'}$

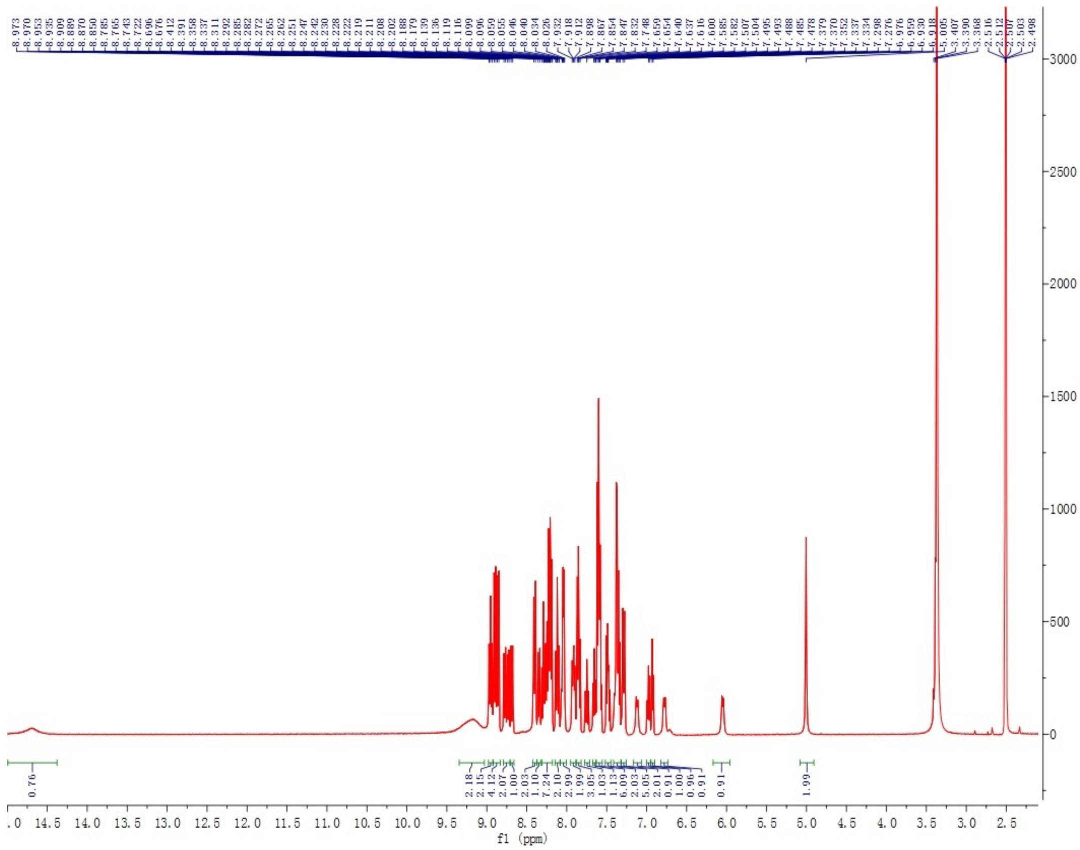

Figure S31. ^{1}H NMR (400 MHz, DMSO-d_6) spectrum of Ru(μ-L^{1}L$^{1'}$)Ru

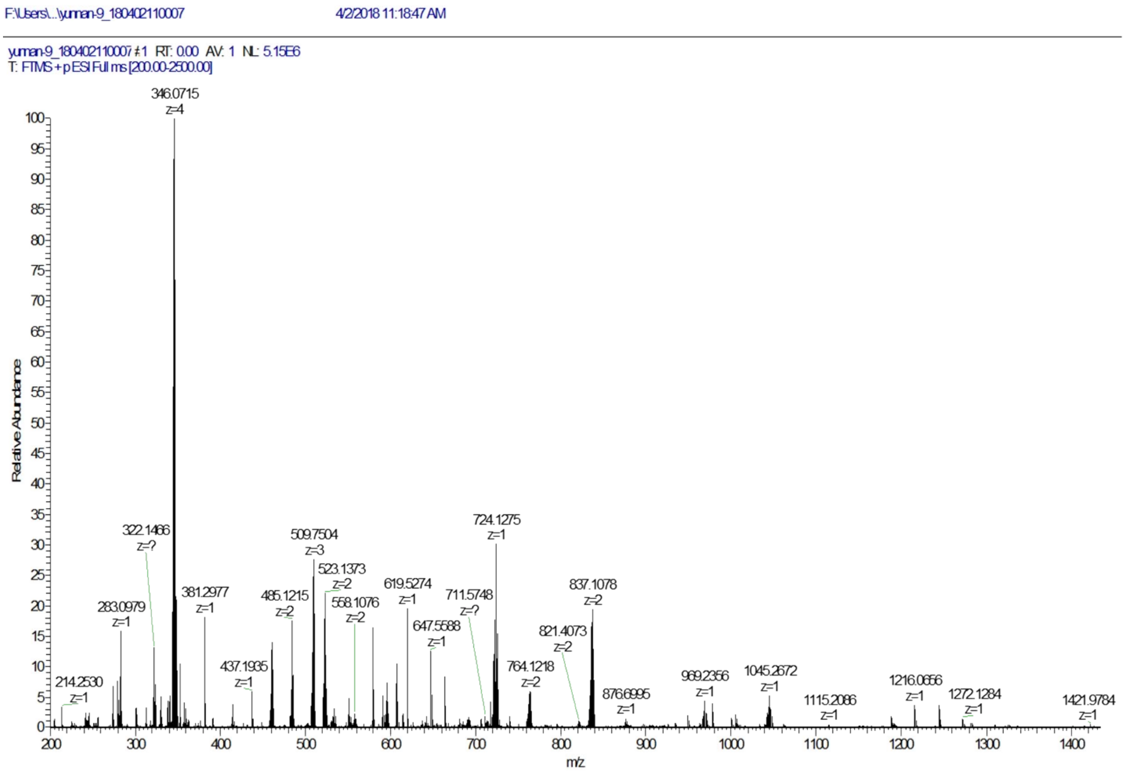

Figure S32. ESI-HRMS of Ru(μ-L^{1}L$^{1'}$)Ru

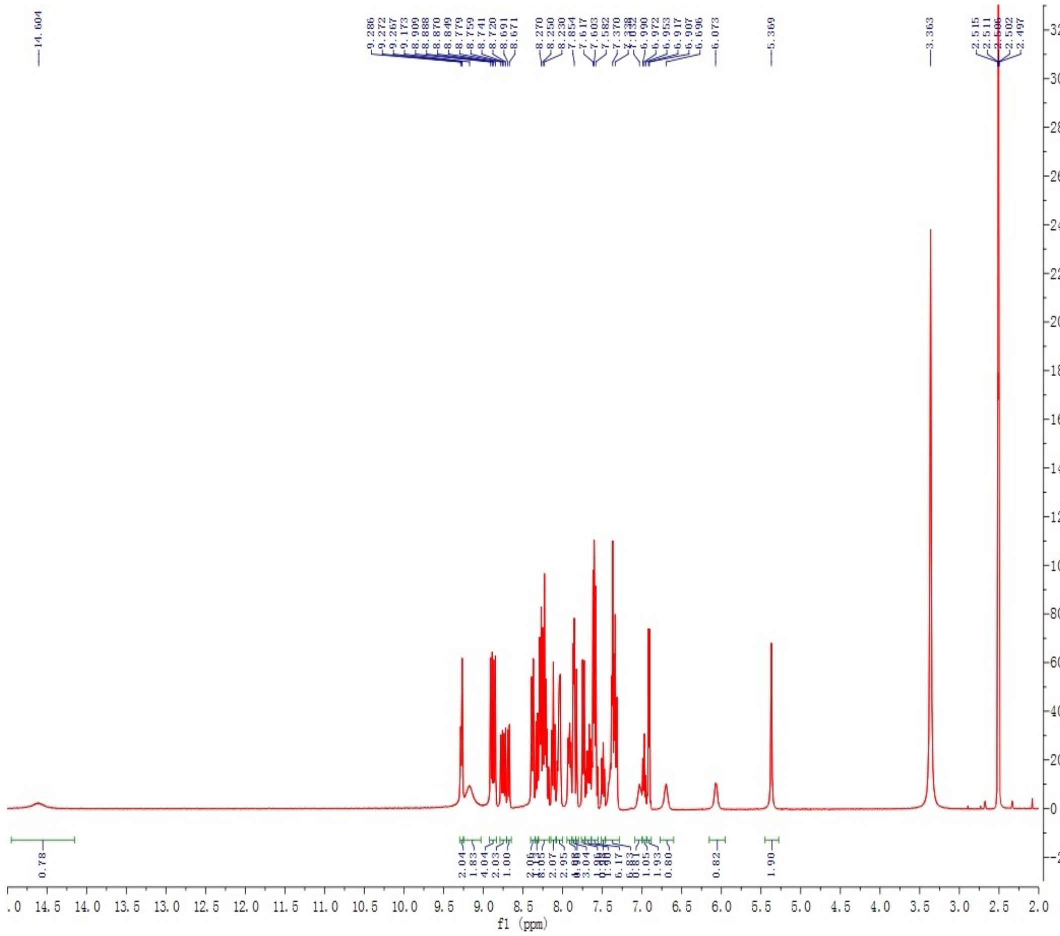

Figure S33. ^{1}H NMR (400 MHz, DMSO-d_6) spectrum of Ru(μ-$L^2L^{2'}$)Ru

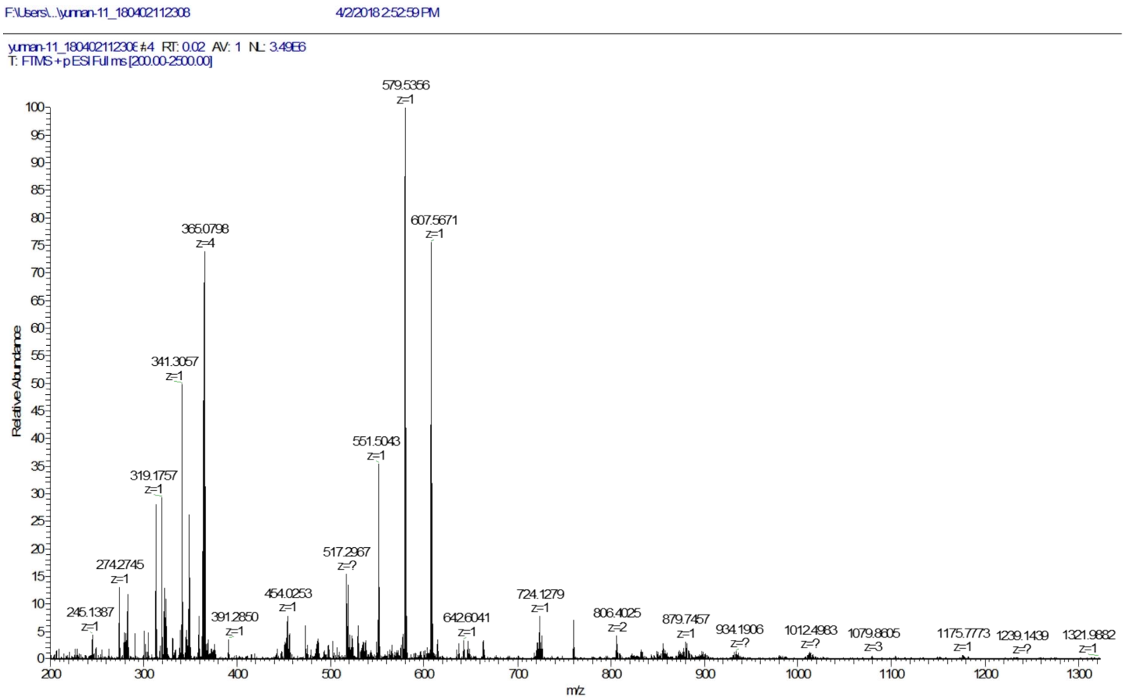

Figure S34. ESI-HRMS of Ru(μ-$L^2L^{2'}$)Ru

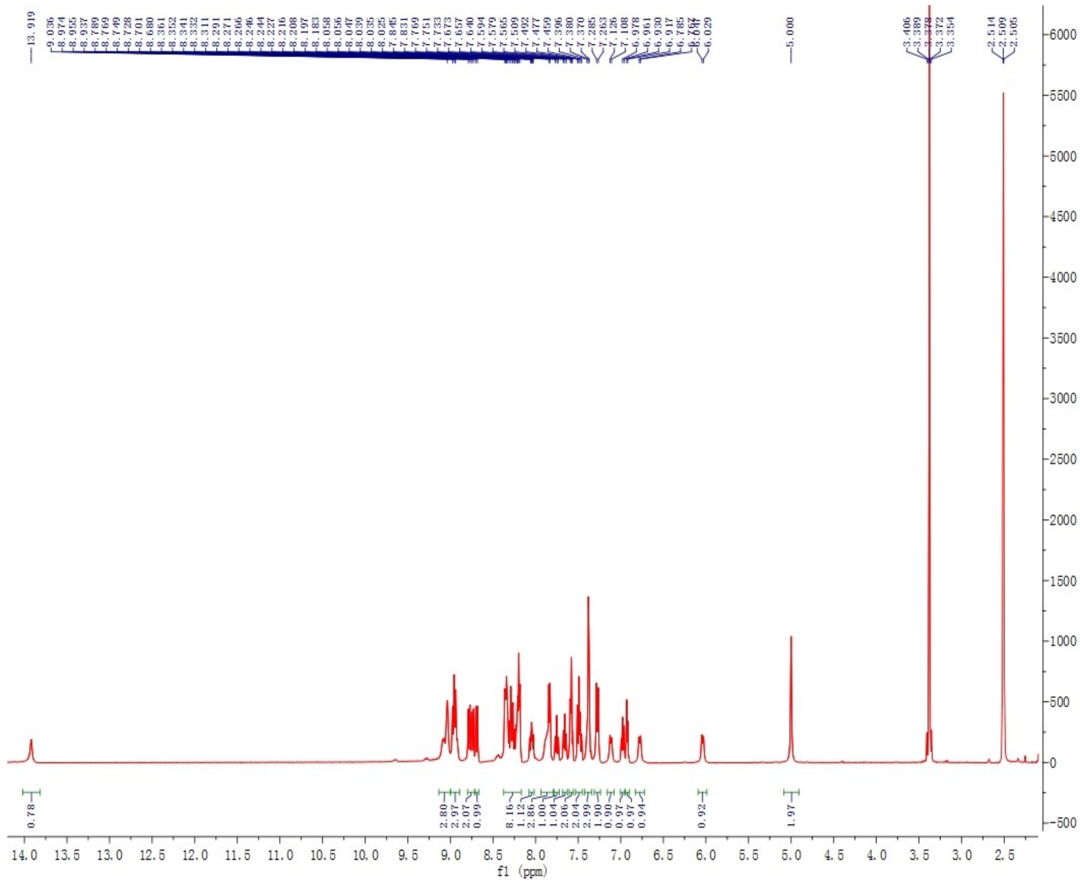

Figure S35. ^1H NMR (400 MHz, DMSO-d_6) spectrum of Ru(μ-L^{1}L$^{1'}$)

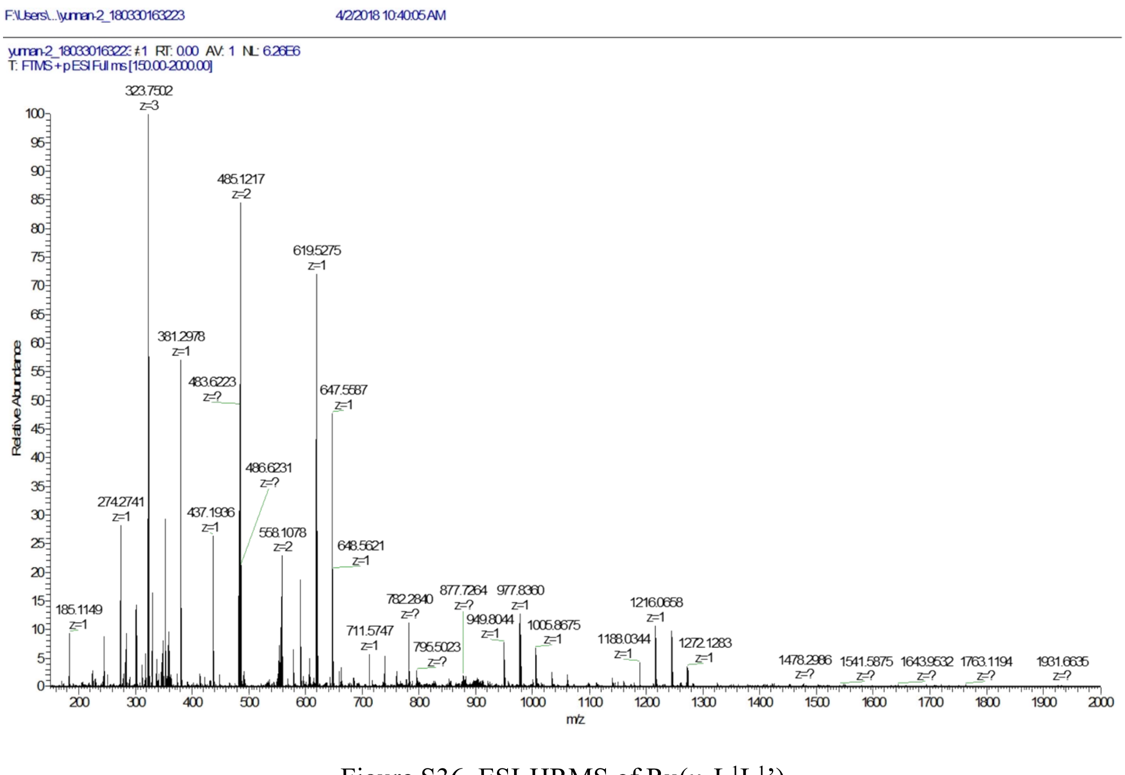

Figure S36. ESI-HRMS of Ru(μ-L^{1}L$^{1'}$)

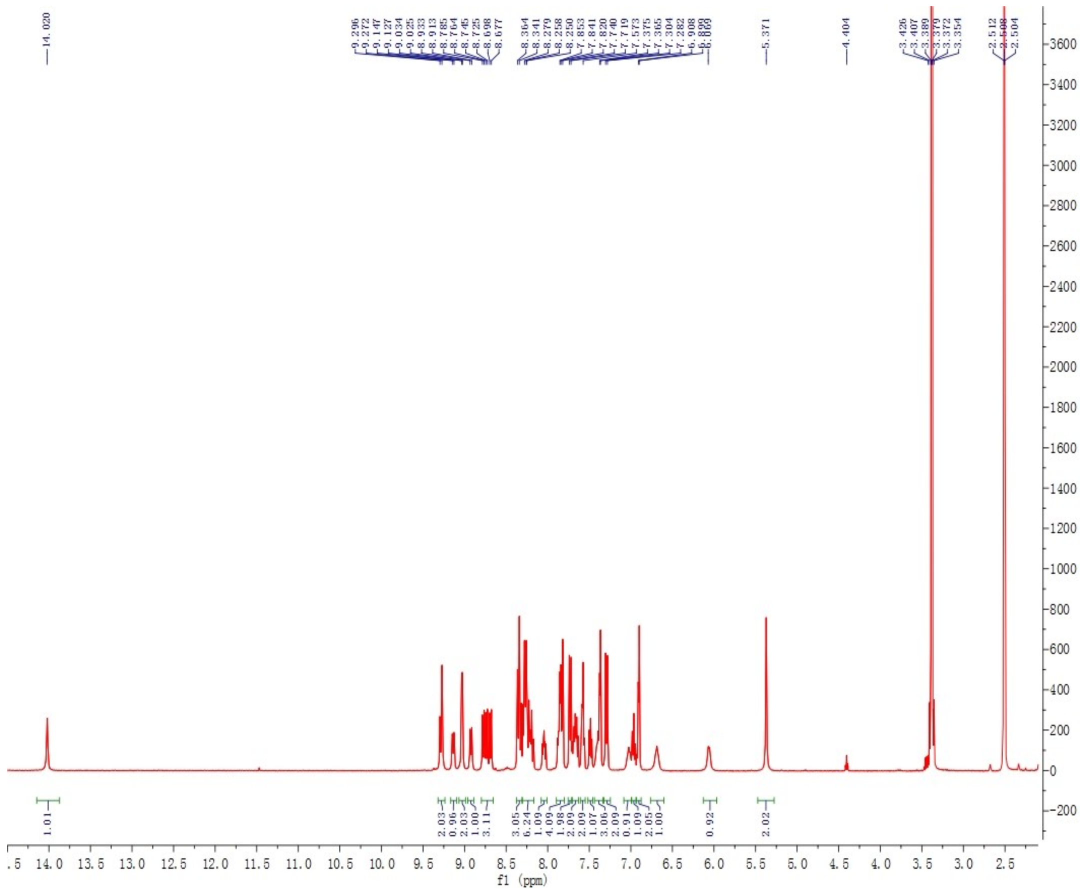

Figure S37. ^{1}H NMR (400 MHz, DMSO-d_6) spectrum of Ru(μ-L^2L^{2}’)

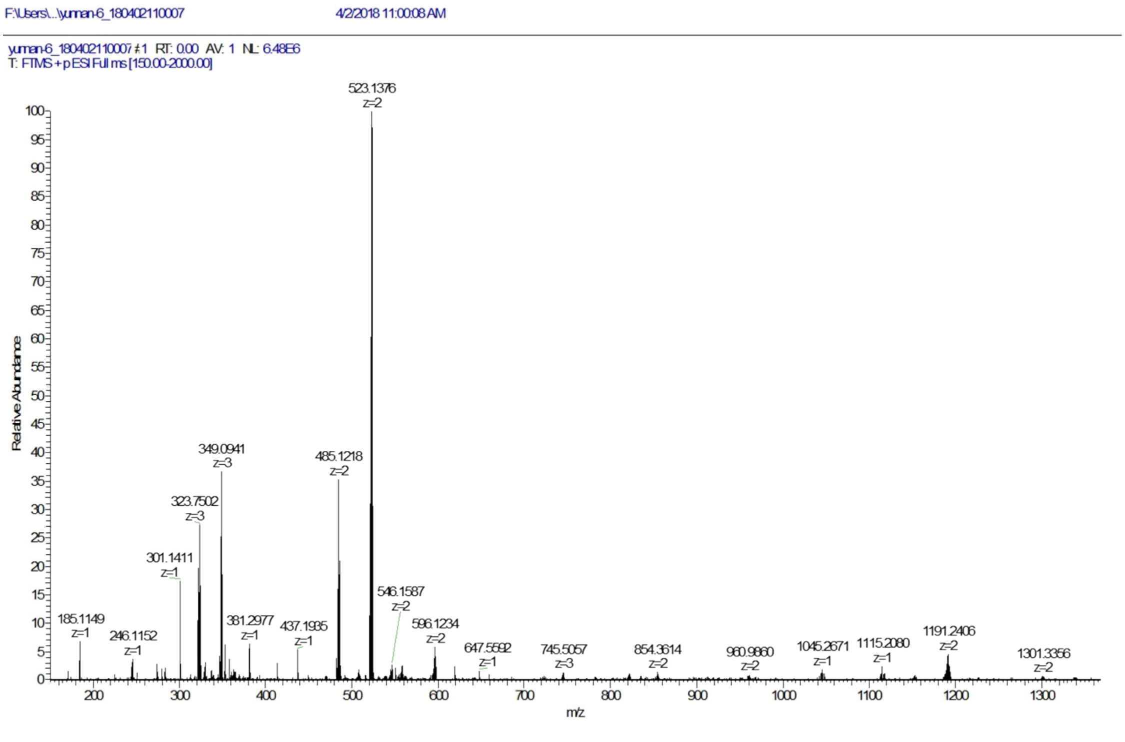

Figure S38. ESI-HRMS of Ru(μ-L^2L^{2}’)

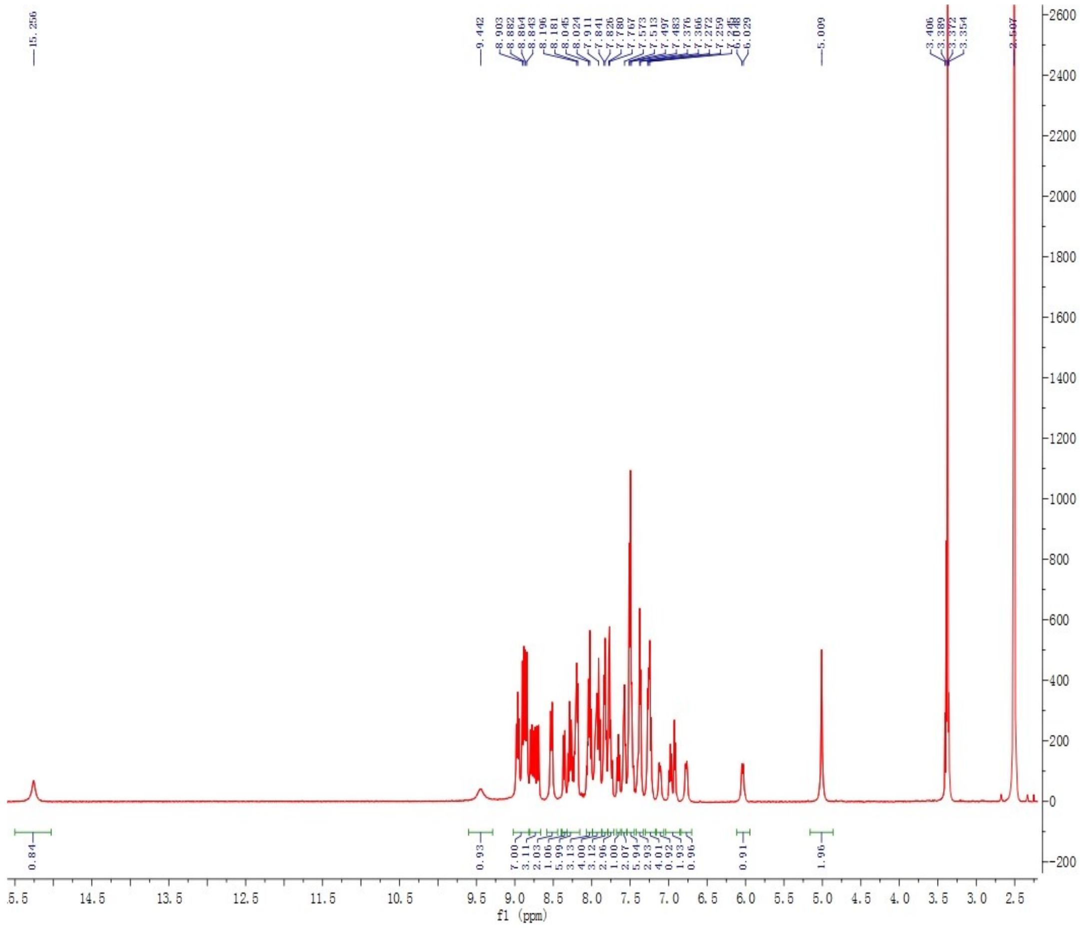

Figure S39. ^{1}H NMR (400 MHz, DMSO-d_6) spectrum of Ru(μ-L^{1}L$^{1'}$)Os

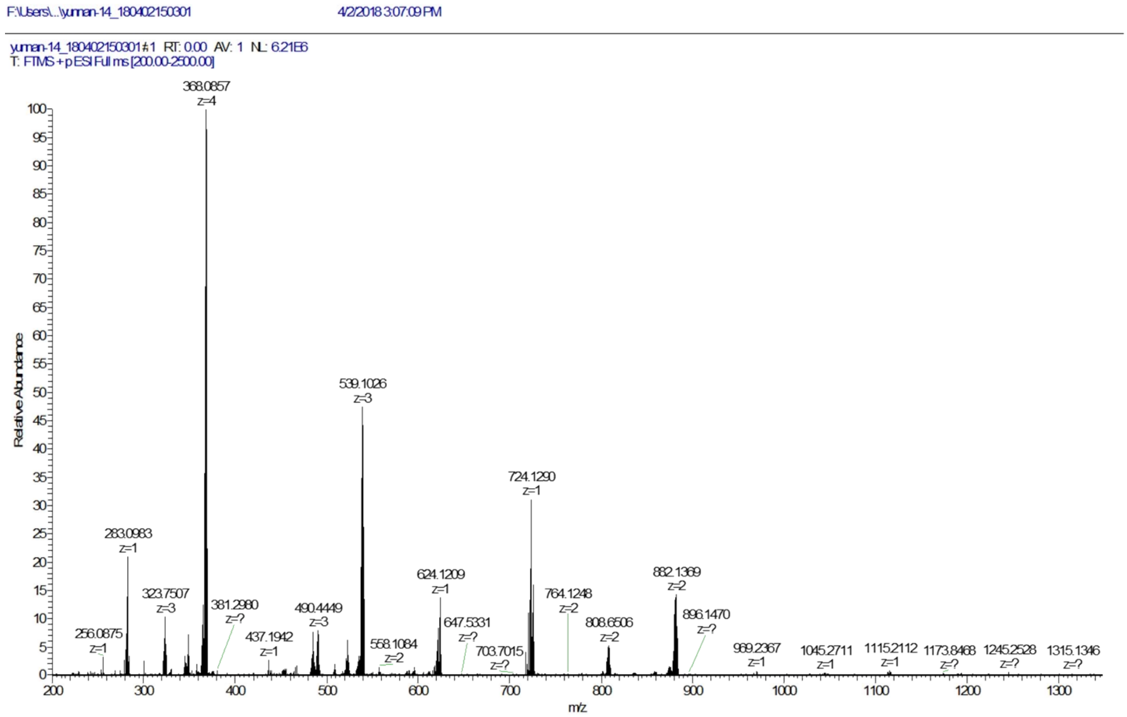

Figure S40. ESI-HRMS of Ru(μ-L^{1}L$^{1'}$)Os

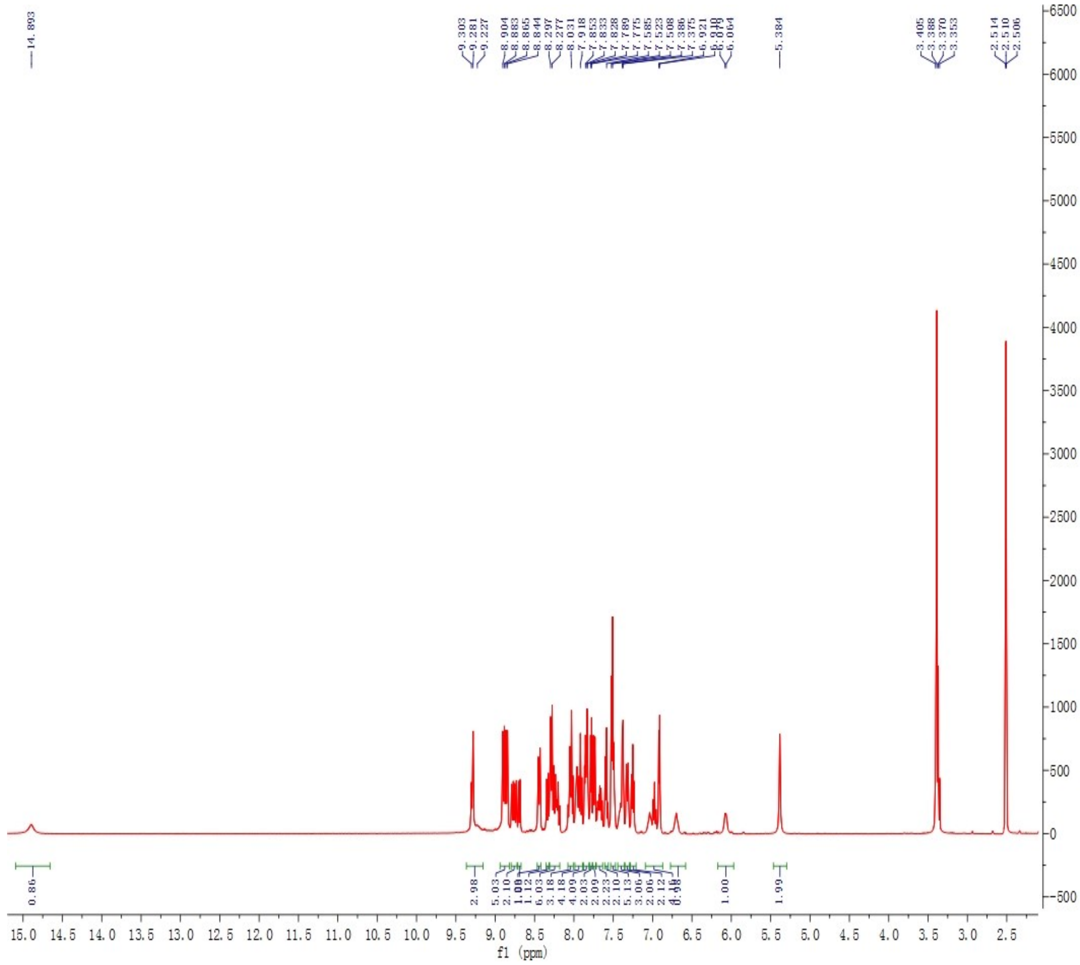

Figure S41. ^{1}H NMR (400 MHz, DMSO-d_6) spectrum of Ru(μ-$L^2L^{2'}$)Os

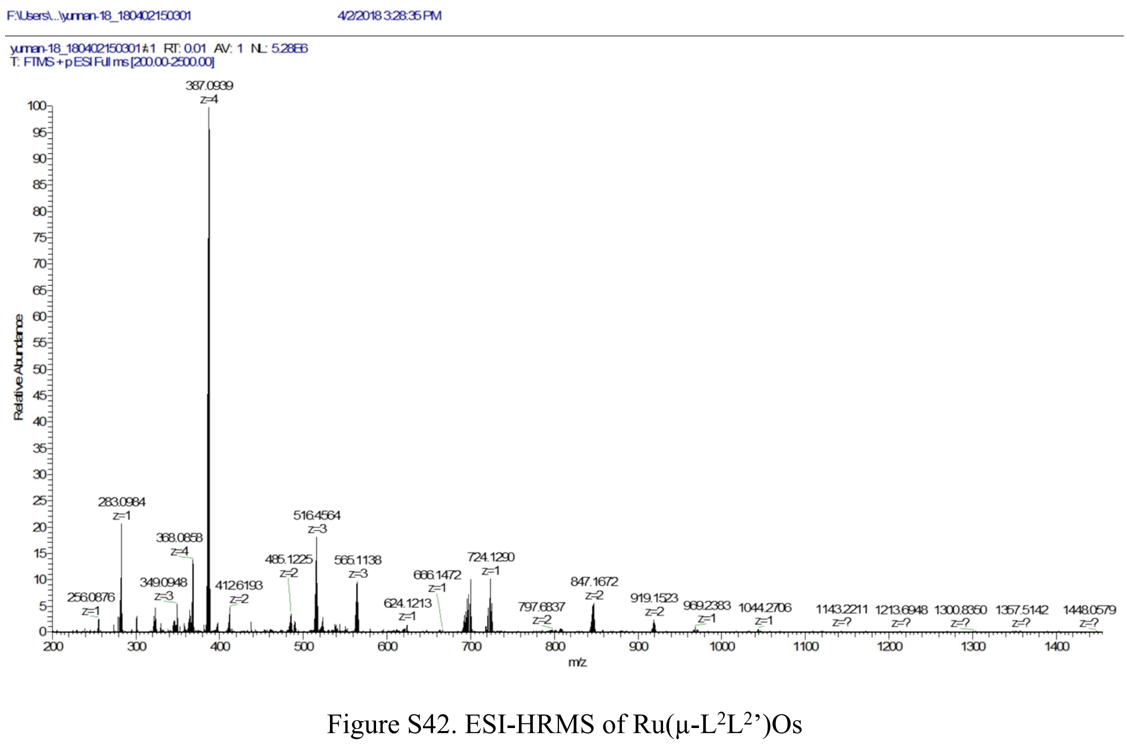

Figure S42. ESI-HRMS of Ru(μ-$L^2L^{2'}$)Os

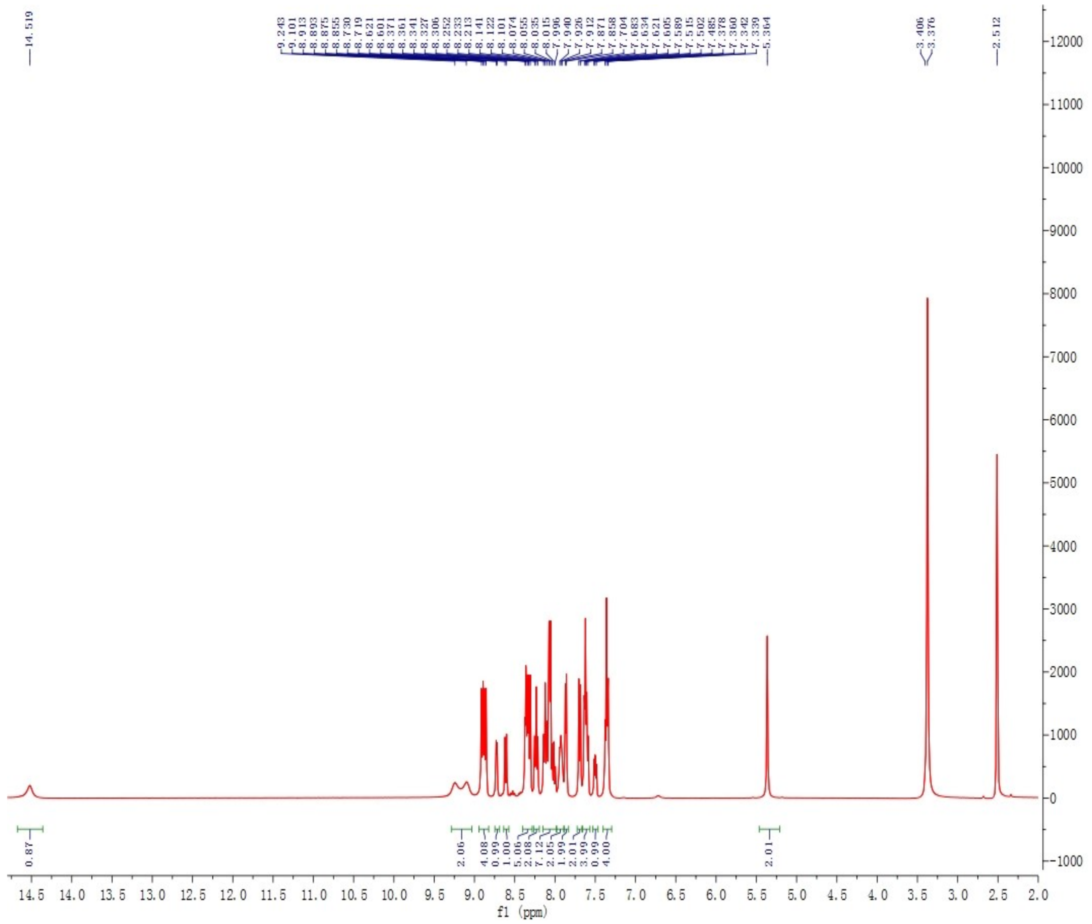

Figure S43. ^{1}H NMR (400 MHz, DMSO-d_6) spectrum of (μ-$L^1L^{1'}$)Ru

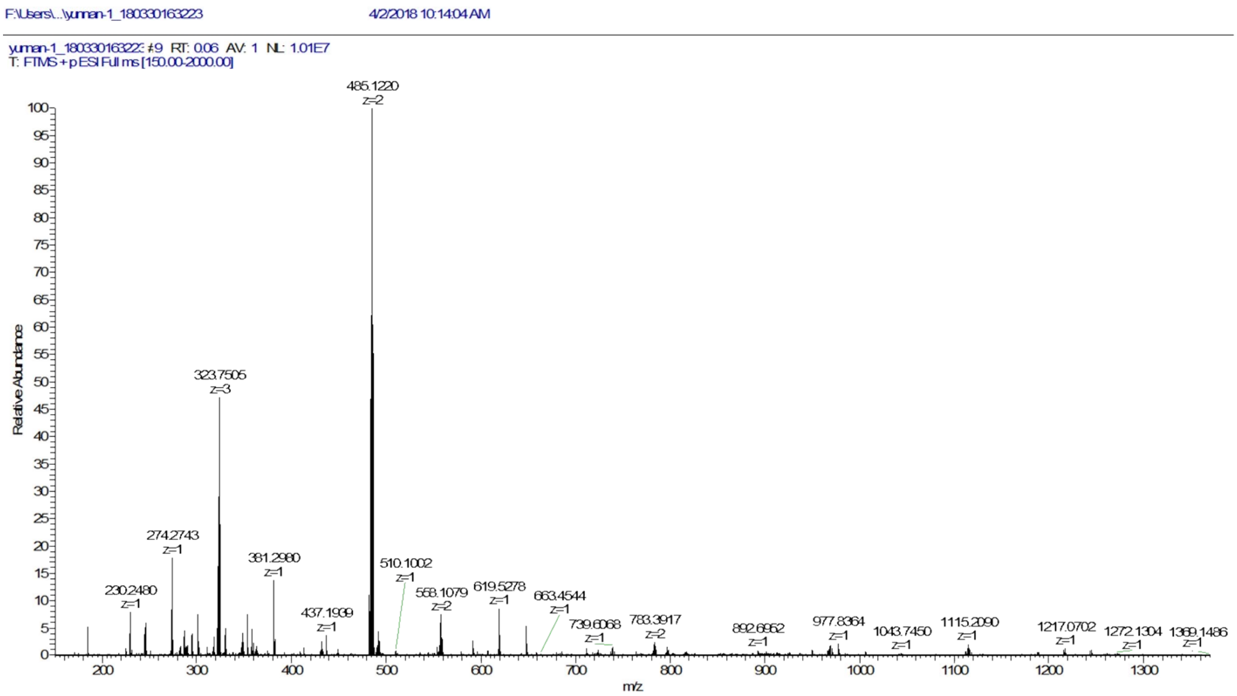

Figure S44. ESI-HRMS of (μ-$L^1L^{1'}$)Ru

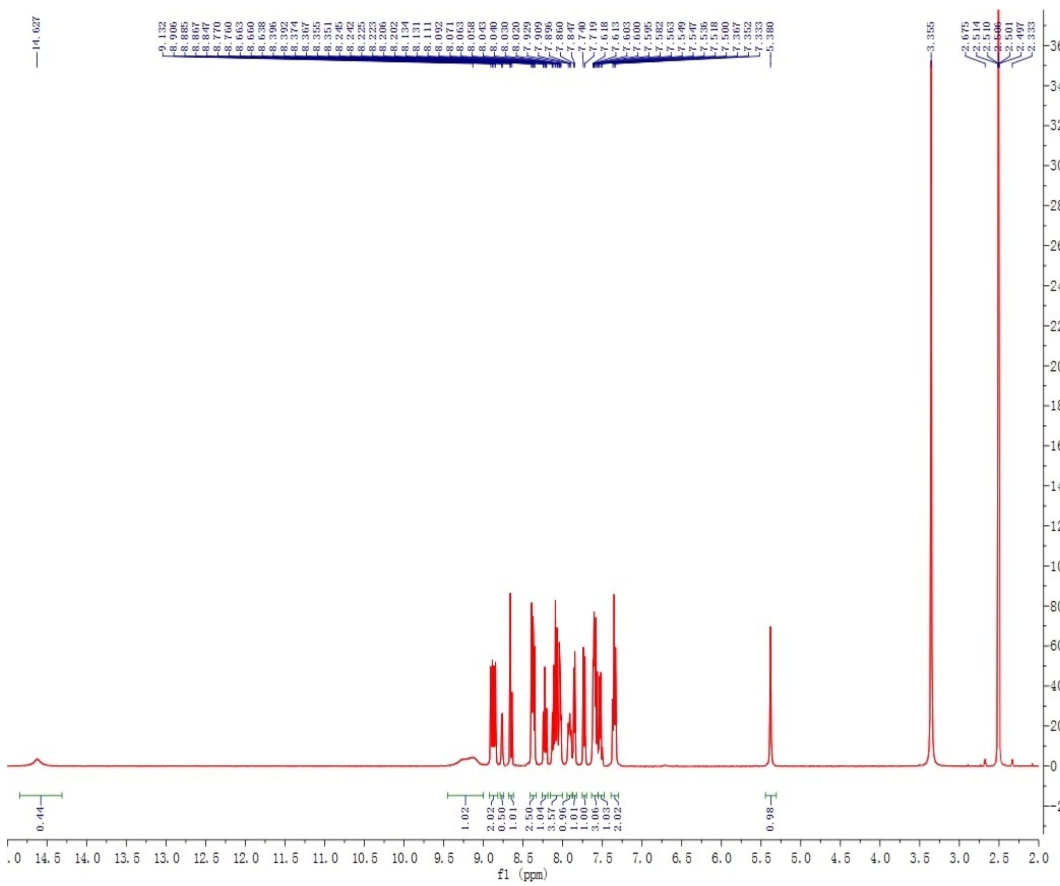

Figure S45. ^{1}H NMR (400 MHz, DMSO-d_6) spectrum of (μ-$L^2L^{2'}$)Ru

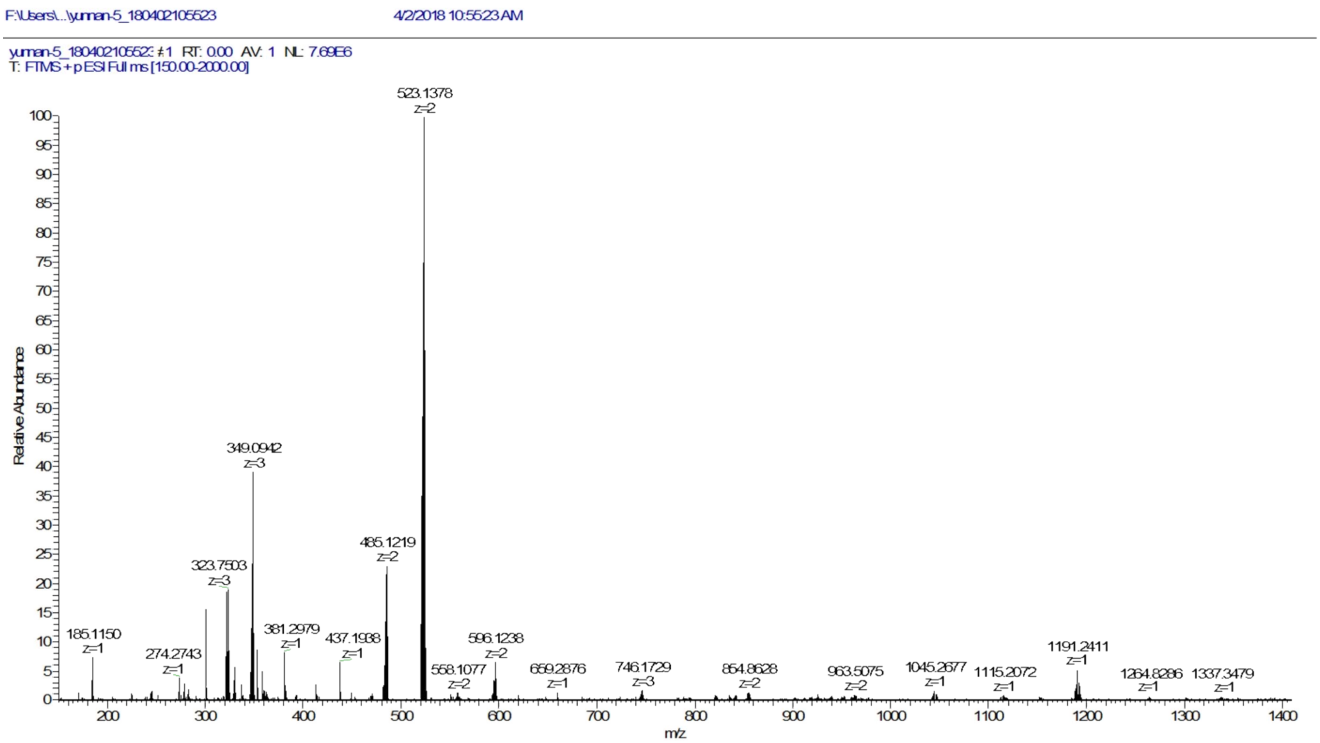

Figure S46. ESI-HRMS of (μ-$L^2L^{2'}$)Ru

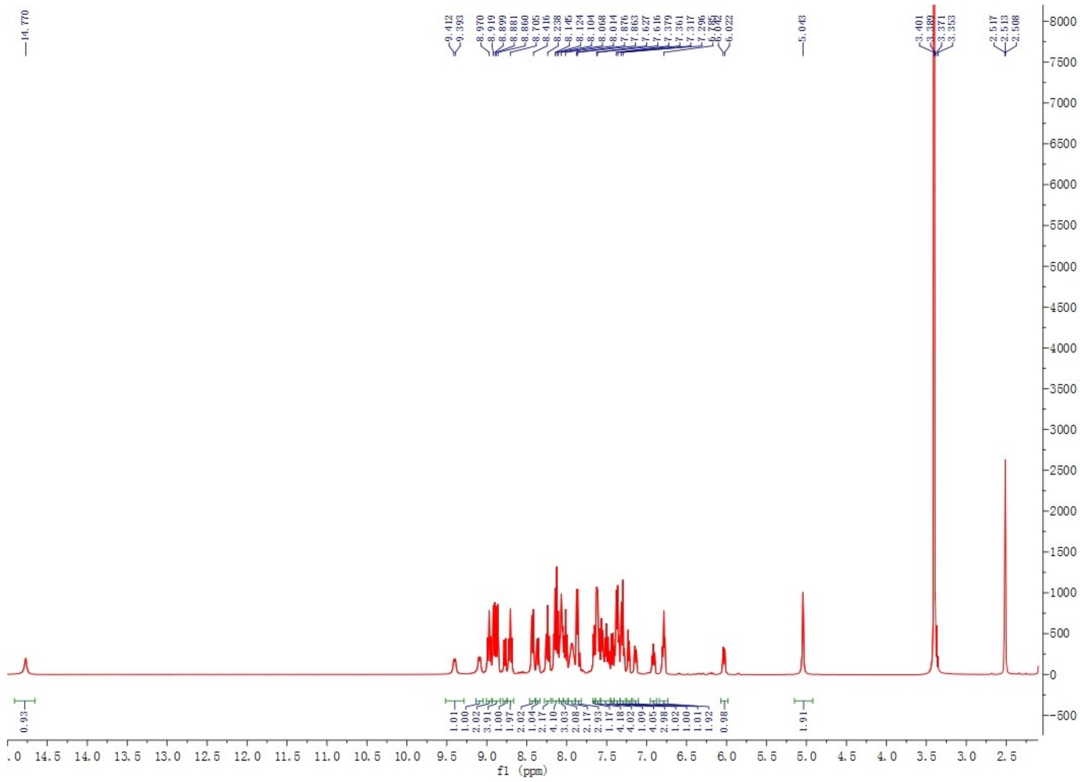

Figure S47. ^{1}H NMR (400 MHz, DMSO-d_6) spectrum of Os(μ-L^{1}L$^{1\prime}$)Ru

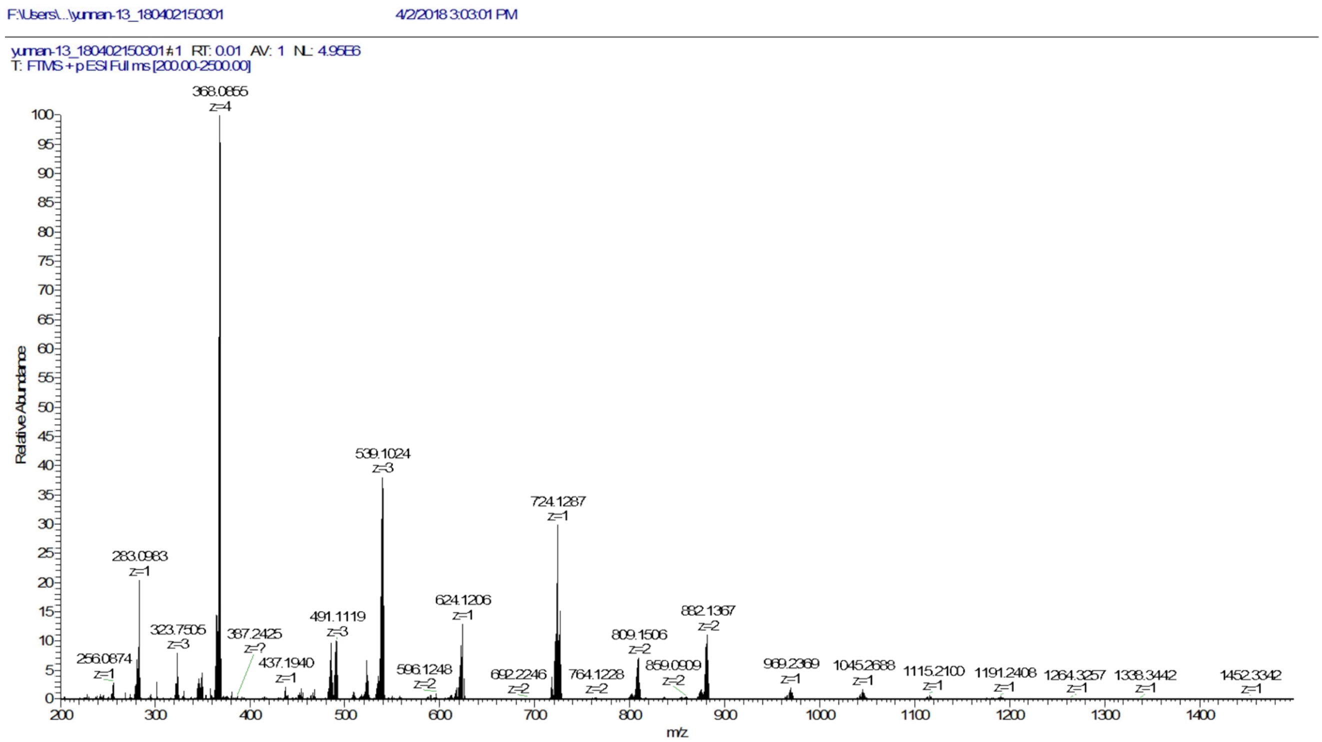

Figure S48. ESI-HRMS of Os(μ-L^{1}L$^{1\prime}$)Ru

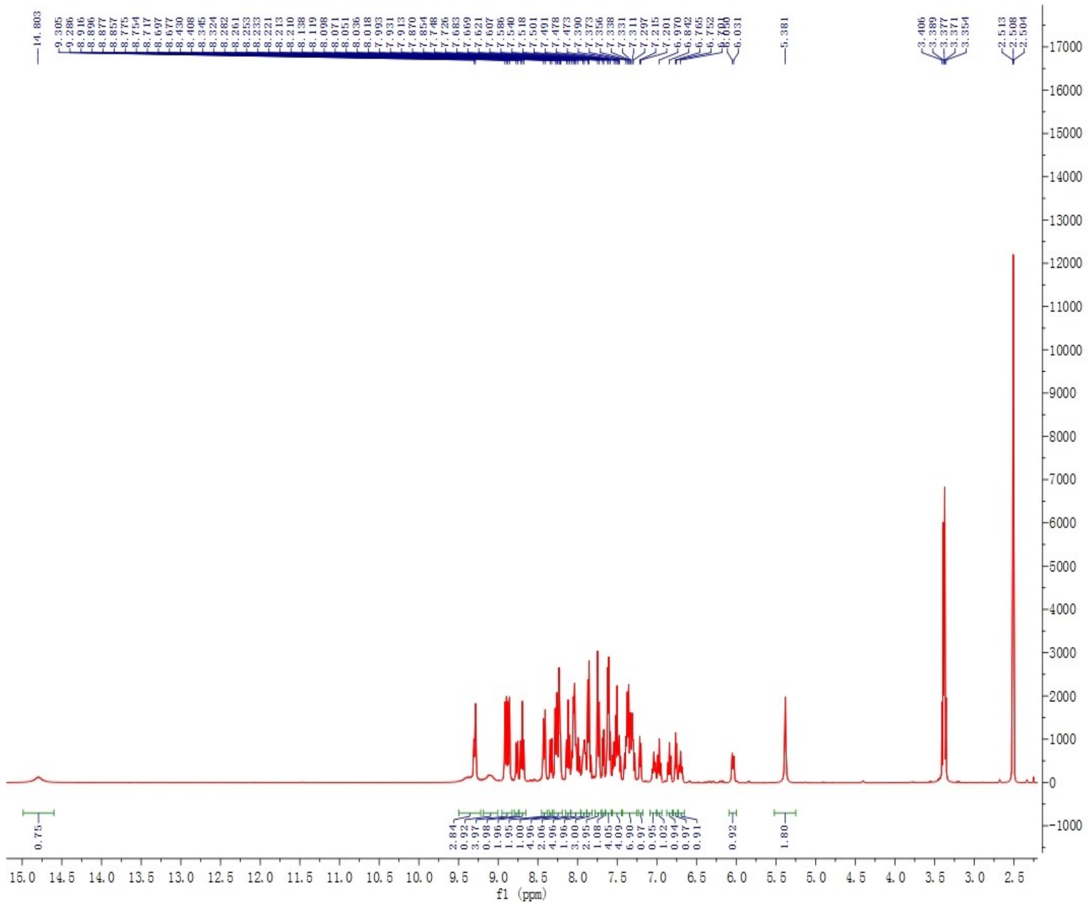

Figure S49. ^{1}H NMR (400 MHz, DMSO-d_6) spectrum of Os(μ-L^2L^{2}’)Ru

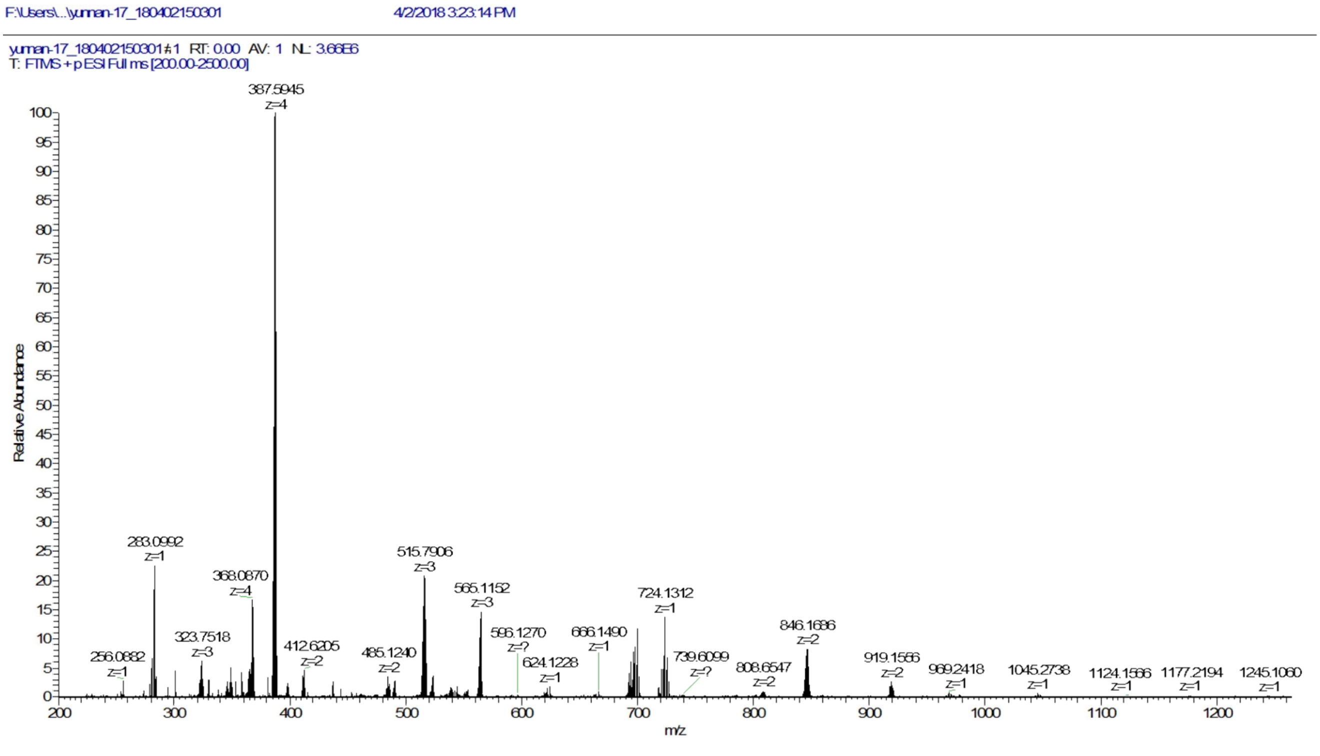

Figure S50. ESI-HRMS of Os(μ-L^2L^{2}’)Ru